Università degli Studi di Napoli "Federico II"

Facoltà di Scienze MM.FF.NN.

Doctorate School in Pure and Applied Physics
XXIII cycle

Anno Accademico 2009/2010

Thesis

Electron-lattice and strain effects in manganite heterostructures

Supervisors:

Prof. V. Cataudella

Dr. C. A. Perroni

Prof. V. Marigliano Ramaglia

Candidate:

Alfredo Iorio

"Bestiali come sempre, carnali, egoisti come sempre, interessati e ottusi come sempre lo furono prima,
Eppure sempre in lotta, sempre a riaffermare, sempre a riprendere la loro marcia sulla via illuminata dalla luce"
(Cori da "La Rocca", T. S. Eliot)

Contents

Introduction

The class of transition metal oxide compounds exhibit a broad range of functional properties, such as high dielectric permittivity, piezoelectricity and ferroelectricity, superconductivity, colossal magnetoresistance and ferromagnetism. Almost all this phenomenology arises from the strong correlation between electronics, which is responsible for the sensitive to external parameters: electric and magnetic fields, internal or external pressure and so on. Nowadays, oxides attracted a large interest in view of device applications, by integrating them in the silicon technology (for instance growing epitaxial high-K oxide films on Si substrates) and in the challenging field of oxide electronics, which aims to develop new electronics based on oxides. Advantages of this new electronics lie in: a) the exploitation of new functionalities exhibited by oxides, which are completely absent in conventional semiconductors, b) the similarity of their structures, which allows the vertical integration of multiple devices through epitaxial heterostructures, c) striking possibility of size reduction due to the nanometric characteristic lengths.

Very recently, high quality atomic-scale "digital" heterostructures consisting of combination of transition metal oxide materials have been realized. Indeed, heterostructures represent the first steps to use correlated oxide systems in realistic devices. Moreover, at the interface, the electronic properties can be drastically changed in comparison with those of the bulk. Recent examples include the formation of a thin metallic layer at the interface between band and Mott insulators as, for example, between $SrTiO_3$ (STO) and $LaTiO_3$ oxides (1) or between the band insulators (2) $LaAlO_3$ and STO.

Among transition metal oxides, manganese oxides $R_{1-x}A_xMnO_3$ (R stands for a rare earth as La, A represents a divalent alkali element such as Sr or Ca and x the hole doping), known as manganites, have been studied intensively both for their very rich phase diagram and for the phenomenon of *colossal* magnetoresistance (3). This effect is often exhibited in the doping regime $0.2 < x < 0.5$, where the ground state of the systems is ferromagnetic. The ferromagnetic phase is usually explained by invoking the double exchange mechanism in which hopping of an outer-shell electron from a Mn^{3+} to a Mn^{4+} site is favored by a parallel alignment of the core spins (4). In addition to the double-exchange term that promotes hopping of the carriers, a strong interaction between electrons and lattice distortions plays a non-negligible role in these compounds giving rise to formation of polaron quasi-particles (5).

The physics of manganites is very rich and even more complex in the case of films, where the role of vertical confinement, strain and disorder is crucial (6). In particular, the interface between the films and the substrate can play an important role giving rise to phase separated regions with different magnetic structures and affecting the transport properties especially in very thin films. Recently, a number of experimental observations in thin films have been reported showing an unexpected strong anisotropy in the in-plane properties (7; 8; 9) below the metal-insulator transition. For very thin films (thickness $< 100\mathring{A}$) of $La_{1-x}Sr_xMnO_3$ (LSMO), grown on different substrates, the resistance curves $R(T)$, along the ab crystallographic axes, have been found remarkably different. In particular, along one of the crystallographic directions, the $R(T)$ curve exhibits a "bump" at temperatures around $120K$ while, along the other one the behaviour of the resistivity appears very close to the one expected for thicker films and bulk samples: metallic up to $320K$. On the other hand, for thick ($> 400\mathring{A}$) films, the resistance curves in different directions of the ab plane did not show sizable differences. The observed anisotropy in the resistance has been attributed to the substrate interface that can exhibit step-like terraces (9; 7). However, the

persistence of the effect with changing the substrate makes this suggestion doubtful.

Very interesting examples of heterostructure are given by the superlattices $(LaMnO_3)_m/(SrMnO_3)_n$ with $n/(m+n)$ average hole doping. Here $LaMnO_3$ (LMO) (one electron per Mn e_g state) and $SrMnO_3$ (SMO) (no electrons per Mn e_g state) are the two end-member compounds of the alloy $La_{1-x}Sr_xMnO_3$ and are both antiferromagnetic insulating. In these systems, not only the chemical composition but also the thickness of the constituent blocks specified by m and n is important for influencing the properties of superlattices. Focus has been on the case $m = 2n$ corresponding to the average optimal hole doping $x = 1/3$. (10; 11) The superlattices exhibit a metal-insulator transition as function of temperature for $n \leq 2$ and behave as insulators for $n \geq 3$. The superlattices undergo a rich variety of transitions among metal, Mott variable range hopping insulator, interaction-induced Efros-Shklovskii insulator, and polaronic insulator.

Interfaces play a fundamental role in tuning the metal-insulator transitions since they control the effective doping of the different layers. Even when the system is globally insulating $(n \geq 3)$, some nonlinear optical measurements suggest that, for a single interface, ferromagnetism due to double-exchange mechanism can be induced between the two antiferromagnetic blocks (12). Moreover, it has been found that the interface density of states exhibits a pronounced peak at the Fermi level whose intensity correlates with the conductivity and magnetization (13). These measurements suggest the occurrence the possibility of a two-dimensional half-metallic gas for the double-layer (14) whose properties have been studied by using ab-initio density functional approaches. However, up to now, this interesting two-dimensional gas has not been experimentally assessed in a direct way by using lateral contacts on the region between the LMO and SMO blocks.

In analogy with thin films, strain is another important quantity in order to tune the properties of manganite heterostructures. For example, far from interfaces, inside LMO, electron localization and local strain favor antiferro-

magnetism and e_g $(3z^2 - r^2)$ orbital occupation (15). The magnetic phase in LMO is compatible with the C type. Moreover, by changing the substrate, the ferromagnetism in the superlattice can be stabilized (16).

In this thesis the electron-lattice and strain effects are analyzed in manganite heterostructures.

In first chapter, the electron reconstruction at surface and interface of correlated electron material is discussed. In particular, some key issues such as strain fields, interdiffusion, etc. in correlated heterostructures are highlighted. The effects of these controlling factors are specialized to manganite heterostructures.

In the second chapter of the thesis, the effects of substrate-induced strain are analyzed in manganite thin films (17). It is proposed that an alternative explanation for the peculiar experimentally observed anisotropy can be based on the formation of *magnetic-stripe* phases (MS). In MS phases the order of t_{2g} spin is such that ferromagnetic stripes alternate with opposite magnetization. The stability of such a phase is discussed without assuming any extrinsic effect at the interface with the substrate. The magnetic physical origin of the observed anisotropy stems from several experimental observations that suggest the existence of a "dead layer", at the interface with the substrate, exhibiting an insulating non-ferromagnetic behaviour (18; 19). A further insight into the problem comes from the well-known observation that these compounds exhibit a strong tendency towards ferromagnetic and antiferromagnetic nanoscopic phase separation (20; 21). Finally, it is worth noticing that the possible existence of extrinsic effects can work as a further stabilizing factor for the magnetic phase we discuss.

The numerical comparison with the isotropic phases (ferromagnetic and G-type antiferromagnetic phases) allows to build up a phase diagram in the plane defined by the transfer integral (hopping amplitude) between nearest-neighbour sites, t, and temperature, T. The hopping amplitude plays an important role since its variations are able to model the presence of strain in the film. Phase diagrams are obtained for different thicknesses. The

stability region for the anisotropic phase moves slightly towards larger values of t with increasing the film thickness and reaches a saturation limit around 100 planes. At the same time, for small values of T the magnetic-stripe phase becomes wider. The film-resistivity has also been calculated as function of the temperature at fixed values of hopping, for different sizes, recovering the in-plane anisotropy observed in the experiments. The anisotropy is obtained when the transition from ferromagnetic to magnetic-stripe phase takes place.

In the third chapter, phase diagrams, spectral and optical properties are discussed for a very large bilayer $(LMO)_{2n}/(SMO)_n$ (up to size of 48 planes allowing for a comparison with fabricated heterostructures) starting from a tight binding model (22). A correlated inhomogeneous mean-field approach has been developed taking into account the effects of electron-lattice anti-adiabatic fluctuations. Strain is simulated by modulating hopping and spin-spin interaction terms. It is found that a metallic ferromagnetic interface forms for a large range of the electron-lattice couplings and strain strengths. For this regime of parameters, the interactions are able to change the size of the interface region. A general structure with three phases running along growth z-direction is found: antiferromagnetic phase with localized/delocalized (depending on the model parameters) charge carriers inside LMO block, ferromagnetic state at the interface with itinerant carriers, localized polaronic G-type antiferromagnetic phase inside SMO block. The type of antiferromagnetic order inside LMO depends on the strain induced by the substrate.

The spectral and optical properties corresponding to different parameter regimes are discussed. Due to the formation of the metallic interface, the density of states is finite at the chemical potential. With increasing the electron-phonon interaction, it gets reduced at the chemical potential, but it never vanishes even in the intermediate to strong electron-phonon coupling regime. Finally, we have studied both the in-plane and out-of-plane optical conductivities pointing out that they are characterized by marked differences: the former shows a metallic behavior, the latter a transfer of spectral weight

at high frequency due to the effects of the electrostatic potential well trapping electrons in LMO block. The in-plane response at low frequency is mainly due to the region between the two insulating blocks, so that it can be used as a tool to assess the formation of the metallic ferromagnetic interface.

Chapter 1

Electron reconstruction at surfaces and interfaces of correlated electron materials

The intellectual challenges posed by *correlated electron* materials (those classes of compounds which exhibit interesting and unusual electronic behavior such as colossal magnetoresistence, high temperature superconductivity, magnetic, charge and orbital order, "heavy fermion" behavior, quantum criticality, etc) are a central focus of condensed matter physics. It is generally accepted that the unusual behavior is due to in large part to strong electron-electron interactions, whose effects cannot be adequately represented by density functional band theory techniques. Over the past decade our understanding of the bulk properties of correlated electron materials has dramatically improved (23). A fundamental observation has been that in bulk, correlated electron materials exhibit a wide range of novel phases, involving various permutations of metallic and insulating behavior, and of superconducting, magnetic, charge and orbital order. It is argued here that the time is now ripe for a systematic investigation correlated electron surface/interface, i.e. of the changes in correlated electron behavior which may occur near the surface of a correlated electron compound or in the vicinity of an interface between a correlated

electron material and another material (either strongly correlated or not). It is further argued that just as the fundamental question in traditional surface science is of surface reconstruction, in other words, of how atomic positions differ on the surface relative to bulk, so the fundamental question of correlated electron surface/interface science is *electronic reconstruction*: how the rich and interesting electronic phase behavior characteristic of the correlated electron materials changes near a surface or interface.

The issue of the surface and interface induced changes in correlated electron behavior is of fundamental interest as a basic question in condensed matter physics and materials science, but is also important from other points of view. The possibility of exploiting the unusual properties of correlated electron systems to make novel devices has intrigued workers for many years; for example, an important motivation for the study of colossal magnetoresistence manganites has been the possibility of exploiting the very high degree of spin polarization in some kind of *spin valve* device (24). However, almost any prospective device involves an interface through which electrons pass; an understanding of the factors controlling the near-interface behavior of correlated electron compounds is therefore essential to rational design and optimization of possible devices. Similarity, there has been much discussion recently of *correlated electron nanostructures* and *correlated electron nanoparticles*. But by definition, nanostructures and nanoparticles posses a very large surface to volume ratio, their electronic properties are likely to be determined by surface effects.

In this work the focus will be mainly on transition metal oxides, because an impressive body of controlled experimental data is accumulating and interesting effects have been revealed. Surface science is a very well developed subject, and much important work on surfaces of transition metal oxides has been done (25). The field of correlated electron surface science is however still in its infancy. Only recently has systematic experimental attention been focused on the surface or interface-induced changes in the novel electronic properties which make the correlated electron materials so interesting (26),

and only recently have appropriate theoretical techniques (27) become available.

A very interesting example of heterostructures has been given by Adamo (28) et al., which have systematically investigated the temperature dependence of the transport properties of $(SMO)_n(LMO)_{2n}$ superlattices with different values of n ($n = 1, 2, 3, 4, 5, 6, 8, 16$). Here n denotes the number of pseudocubic unit cells comprising the thickness of each SMO layer in the superlattices. due to the very low spatial disorder of the used samples, they have been observed several transitions from metal to insulator as function of n and temperature (See Fig. 1.1). Such a variety of transport regimes, observed at very different dopings in an A-site alloy, can be tuned at changing only the interface number. These analysis point out the fundamental role played by interfaces in clean layered systems. This effect is relevant even in the case of a single interface, where an electronic reconstruction nucleates at the interface.

1.1 Controlling factors

The central physics of transition metal oxide compounds is the "Mott" metal insulator transition occurring at commensurate band fillings and associated with magnetic, charge and orbital order. The basic questions, therefore, are how the Mott insulating behavior differs at the surface from the bulk, and whether the associated magnetic, charge and orbital ordering patterns (if any) are the same at a surface or interface as they are in the bulk, or different.

Important factors controlling the Mott physics include carrier concentration, relative strength of interaction and band width, orbital degeneracy and disorder. These are changed by proximity to a surface or interface. Some key issues include:

- *Strain fields*, induced by lattice mismatch at an interface or by reconstruction at a surface: these may extend a long distance from a surface

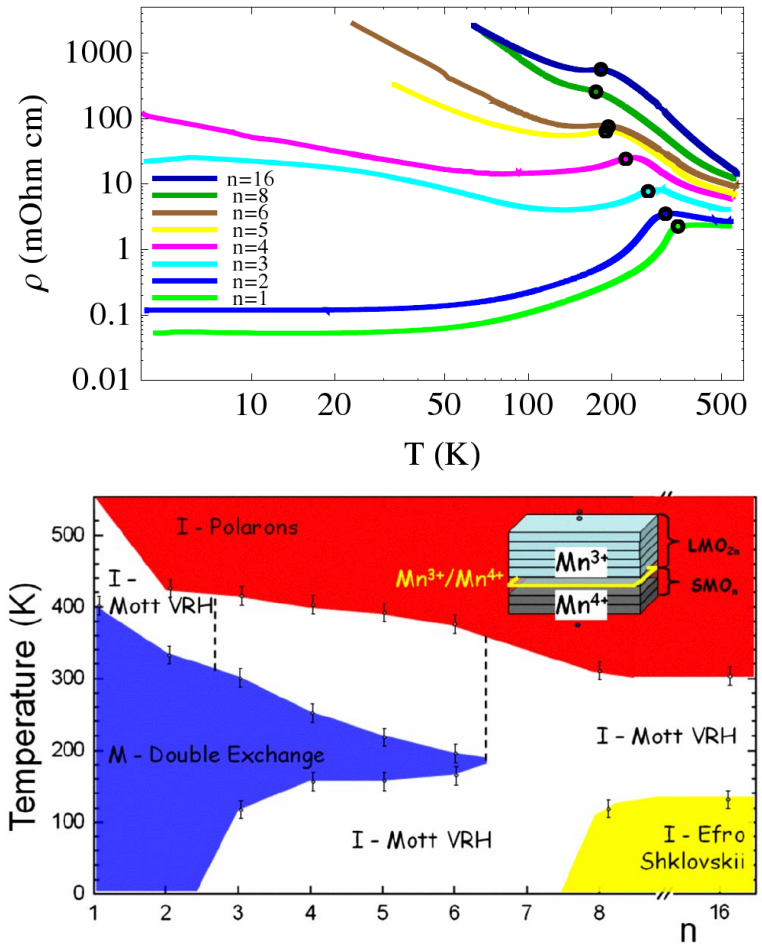

Figure 1.1: (Upper panel) The measured resistivity as a function of temperature for several values of n. The circles mark the experimental Curie temperatures which are always very close to T_{MI}. (Lower panel) The cartoon summarizes all the different transport regimes obtained changing n. M stands for metal, I stands for insulator, and VRH for variable range hopping.

or an interface, and act to lift orbital degeneracy and also to change hopping amplitudes.

- *Interdiffusion* of atoms across an interface may be an important source of disorder: expecially in heterostructures composed of different types of transition metal oxides, the chemical similarity makes it difficult to prevent interdiffusion, while the different physical properties associated with different transition metals implies that the associated disorder will be very large.

- *Atomic reconstructions*: electronic band-width is controlled by the interatomic distance and by the geometrical arrangement of atoms, both of which may change because the structure of the surface (or sometimes an interface) may be reconstructed relative to bulk, while interaction strength is strongly affected by the polarizability of surrounding ions which may also change near a surface or an interface.

- *Surface charge layers*, due for example to the need to compensate a polar surface will lead to substantial band-bending and thus to near-surface charge variation.

- *Leakage of carriers* across an interface from one material to another also implies local variation of charge density.

In the following section we summarize recent experimental work relating to each of these phenomena. The identification of well-controlled experimental systems which isolate (to the extent possible) one factor or the other is important, because many factors may contribute to a difference in behavior between surface and bulk, and what is most important in practice may not always be clear a priori.

1.1.1 Strain fields: effects in manganites

Strain Growth of thin $(10-100nm)$ films and heterostructures of interesting oxides on (relatively) inert substrates in an important activity pursued by

many groups world-wide. Most suitable substrates have a significant lattice mismatch with material of interest. This mismatch strains the material of interest, and research over the last five years has made it clear that this strain can strongly affect physical properties, especially of materials, such as *colossal* magnetoresistence manganites, in which orbital degeneracy plays an important role. Early evidence of the importance of anisotropic strain was provided by A. J. Millis et al.(29), who showed via theoretical calculations and ultrasound experiments that an infinitesimal anisotropic strain strongly suppressed the ferromagnetic transition temperature of manganite materials. Subsequently, the University of Maryland group (30) and, independently, the University of Tokyo group (31) showed that substrate-induced *compressive* strain could actually change the ground state of $la_{0.7}Ca_{0.3}MnO_3$ from metallic to insulating. The length scales relevant for strain effects in manganite films appear to be of the order of $0.2 - 40nm$; beyond this length one form of structural defect or another appears, allowing the substrate-induced strain to heal.

The theoretical understanding of these results is not complete. Fang and colleagues (32) presented local spin density approximation band calculations which indicated that compressive strain of this order of magnitude could change the magnetic state from ferromagnetic to antiferromagnetic. However, it is not clear how antiferromagnetism in a partly filled band could produce the observed insulating behavior. In bulk manganite materials, insulating behavior is now known to be due to charge and orbital order (which often, although not always, leads to antiferromagnetism as well). Biswas and co-workers (30) showed that their compressively strained films exhibited a field driven insulator-metal transition with transport properties very similar to those observed in bulk materials with charge and orbital ordering. These results suggest that strain induces a charge and orbitally ordered insulating state, but this state has not yet directly detected and theoretical explorations of the possibility are lacking. The effects of strain on the properties of manganites and other complex oxides is attracting increasing

attention due to the rapidly expanding research interest in complex oxides heterostructures (33). In fact, phase transitions driven by strains have been discussed in manganite thin films for several years. The physical mechanism of these phase transition is mostly orbital-order-mediated (34). For example, according to density functional theory (DFT) calculations, the ground states of $LaMnO_3/SrMnO_3$ superlattices can be tuned between A-type antiferromagnetic phases when the ratio c/a is in the range $0.96 \sim 1.04$, where c (a) is the out-of-plane (in-plane) lattice constant (35). Even for $LaMnO_3$ itself, the ground state may become ferromagnetic (FM) if the $|3x^2 - r^2 > /|3y^2 - r^2 >$ type orbital order is fully suppressed in the cubic lattice, according to both the DFT and model calculations (34).

Recently, a number of experimental observations in thin films have been reported showing an unexpected strong anisotropy in the in-plane properties below the MI transition. For very thin films (thickness $< 100\mathring{A}$) of $La_{1-x}Sr_xMnO_3$ (LSMO), grown on different substrates, the resistance curves $R(T)$, along the ab crystallographic axes, have been found remarkably different (See Fig. 1.2). In particular along one of the crystallographic directions the $R(T)$ curve exhibits a "bump" at temperatures around $120K$ while along the other one the behaviour of the resistivity appears very close to the one expected for thicker films and bulk samples: metallic up to $320K$. On the other hand, for thick ($> 400\mathring{A}$) films, the resistance curves in different directions of the ab plane did not show sizable differences. The observed anisotropy in the resistance has been attributed to the substrate interface that can exhibit step-like terraces. However, the persistence of the effect with changing the substrate makes this suggestion doubtful.

Very recently, Ward et al., have observed high anisotropic resistivities in strained $La_{\frac{5}{8}-x}Pr_xCa_{\frac{3}{8}}MnO_3$ (LPCMO) thin films (36). LPCMO is a prototype phase-separated material (37). The coexistence of FM and charge-orbital-insulating (COI) clusters at the (sub)micrometer-scale can seriously affect the electric transport properties, especially the metal-insulator transition (MIT). The electric conductance in the phase-separated LPCMO is

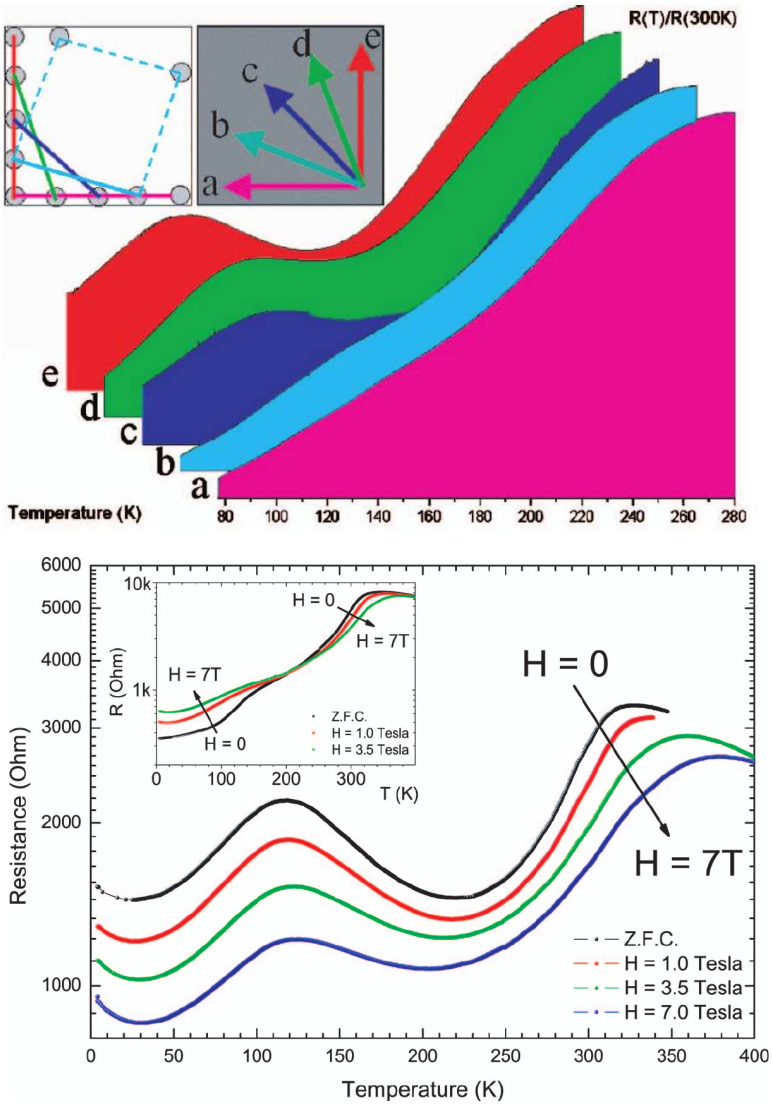

Figure 1.2: (Upper panel) In the inset, the schematic diagram of the Van der Pauw geometrical configurations of the two current injection is reported; aside, the corresponding current flowing direction is sketched using colored arrows. The resistance vs temperature behavior corresponding to the different current direction arrangement for $10nm$-thick LSMO film is reported. (Lower panel) Temperature dependence of resistance as a function of an external magnetic field for the bump configuration(in the inset the no-bump configuration is also reported). The are relative to LSMO film grown on a STO substrate.

dominated by the percolation mechanism (38). For example, giant discrete steps in the MIT and a reemergent MIT occur in an artificially created microstructure of LPCMO when the size confinements in two directions become comparable to the phase-separated cluster sizes (39). Therefore, Ward et al. proposed that the anisotropic percolation might be responsible for the highly anisotropic resistivities in strained LPCMO (36). The results of Monte Carlo simulation (40) shows that the highly anisotropic resistivities are associated with an unbalanced in orbital populations which is driven by the anisotropic double-exchange and anisotropic Jahn-Teller distortions. Therefore, it is expected that this anisotropic state could be realized in a variety of manganites and other complex oxides as well, if a sufficiently large lattice mismatch can be achieved in the growth of the manganite films.

1.1.2 Interdiffusion

Interdiffusion of ions across an interface is a fundamental difficulty in the preparation of heterostructures. The situation is exacerbated in the case of transition metal oxide compounds by the relative similarities in size and chemical bonding tendencies of different transition metals. For example, fabrication of high quality bulk *double perovskite* samples of materials such as Sr_2FeMoO_6 (a high Curie-temperature half-metal which could be very promising for spintronic applications (41)) is severely complicated by tendency towards mis-site disorder (42) (Fe sitting where Mo should and vice-versa). This dramatically degrades the properties and is very difficult to prevent even though Fe is in the $3d$ series and Mo is in the $4d$ series and in a different column of the periodic table.

In recent years the Kawaski group at the University of Tokyo, for example, has undertaken a systematic study of many transition metal oxide superlattices (43) and has presented evidence that interdiffusion of transition metal ions across interfaces fundamentally affects the properties when layers are thinner than about $0.1nm$. Experimentalists however are making continuing impressive progress on the difficult problem of controlling growth

on the atomic scale, and it seems likely that interdiffusion will become less of an issue in the future.

1.2 Atomic reconstruction and other changes near a surface

Atoms near a surface or interface experience a different local environment than those in the bulk of a material, with evident consequences for near-surface electronic behavior. One obvious effect is that the coordination of atoms near the surface is lower than in bulk. The concomitant reduction of net carrier delocalization will tend to increase the effects of correlations. Photoemission studies of $Li/CaVO_3$ (44) and V_2O_3 (45) have been interpreted in this way (46). The effects may be expected to be relatively subtle because the relative change in coordination is often small (1/6 for the (001) surface of a cubic lattice, for example). For this reason some of the theoretical works (47) have argued that a *fine tuning* of a interaction parameter to close proximity to the Mott critical value is necessary to understand the data.

Other effects however also may occur. As noted by Duffy and Stoneham (48) and verified, extended and emphasized by G. A. Sawatzky and collaborators (49), one important consequence of the change in local environment is a change in screening, which leads to change in the effective *Hubbard U* or *charge transfer gap*, which is the crucial interaction parameter controlling the nature of the electronic phase. The change may become larger, for a transition-metal-oxide-normal metal interface or smaller, for a transition metal oxide-vacuum interface.

The difference in local environment between a surface or interface and bulk may lead to changes in positions of near-surface atoms. These changes may lead to a different lattice symmetry at the surface or simply to changes in interatomic distances and bond angles. In either case, changes in near surface electronic structure will result, changing the interplay between band-

width and interaction, and possibly changing the electronic phase. For example, some experimental results (50) report photoemission evidence for a correlation-driven *charge disproportionation* at the surface of $Ca/SrVO_3$ which, it is suggested, may be due to a rotation of the VO_6 octahedra at the surface.

1.2.1 Surface charge layers

One important class of surface (or interface) is the polar surface. Issues associated with polar surfaces are particularly important for strongly correlated transition metal oxides, many of which form in some variant of the simple ABO_3 perovskite structure. For many materials in this structure most of the obvious surface planes (for example, the (001) plane of $LaTiO_3$ are polar in the absence of significant reconstruction relative to bulk. While the conventional expectation is that the charge in balance caused by a polar surface is compensated by atomic surface reconstruction (either a high degree of vacancies or adatoms, or by faceting so the surface is locally nonpolar), it has been proposed theoretically that instead an *electronic reconstruction* many occur, leading for example to a metallic layer at the surface of insulating ZnO. This effect would certainly change correlated electron properties; for example, insulating phases are favored at commensurate densities, and metallic phases at incommensurate densities. G.Sawatzky and collaborators have presented evidence that this behavior occurs at polar surfaces a correlated system (namely K_3C_60).

1.2.2 Charge leakage

At an interface between two different materials, leakage or charge density from one material to the other means that the electronic density near the interface is different from the bulk density in either material. This effect leads, of course, to the Schottky barrier physics essential to semiconductor junctions. It may also have important implications for correlate electron physics,

because the behavior of correlated electron systems depends strongly on the carrier density. Kawasaki and collaborators have presented experimental evidence of the importance of this effect in the context of heterostructures grown of different magnetic transitions metal oxides.

Recent experimental work provides a dramatic illustration of the effects of charge leakage. Ohtomo, Muller, Gredul and Hwang have succeeded in fabricating digital heterostructures $LaTiO_3/SlTiO_3$. $LaTiO_3$ is a "Mott" insulator in which the formal valence is such that there is one d-electron per Ti and La is in the +3 state, whereas $SrTiO_3$ is a band insulator, with (in the formal balance language) no d-electrons per Ti and with Sr in the +2 state. These two materials have essentially identical crystal structures and lattice constants, and in a tour de force of film growth, Ohtomo et al. succeeded in growing a wide range of heterostructures in which an arbitrary (small) number n of $LaTiO_3$ layers alternated with a different, arbitrary number m of $SrTiO_3$ layers. For all heterostructures studied, metallic conduction in the plane of the heterostructures was observed, whereas the bulk material is insulating.

Finally, Ohtomo et al. were able to use the electron energy loss mode of a transmission, electron microscope to map out the distribution of Ti d-electrons significant "leakage" of the Ti d-electron density from the $LaTiO_3$ region to the $SrTiO_3$ region was observed.

Chapter 2

Low temperature magnetic and transport anisotropy in manganite thin film

In this chapter the studying on the magnetic and transport anisotropy in $La_{1-x}A_xMnO_3$ thin films is presented. The stability of striped magnetic phases in films of $La_{1-x}A_xMnO_3$ perovskites is investigated. A variational analysis is developed for different film thicknesses at fixed hole density ($x = 0.3$) and the competition among magnetic phases as a function of the transfer integral and the temperature is analysed. The stabilization of an in-plane striped magnetic phase is observed with reducing the film thickness at low temperatures below the metal-insulator transition temperature. Within the adopted variational scheme, treating perturbatively the residual electron-phonon interaction, the dependence of the in-plane resistivity on temperature for different thicknesses is calculated. At low temperatures, due to the striped magnetic phase, the resistivity shows an important in-plane anisotropy. The obtained results are found to be consistent with experiments.

2.1 The model and the variational approach

The so-called single orbital approximation for manganite is adopted. This model, qualitatively accurate for $x < 0.5$, describes the dynamics of the e_g electrons subjected to the double-exchange mechanism and coupled to the lattice distortions. It also takes into account super-exchange interaction between neighbouring localized t_{2g} electrons. The coupling to longitudinal optical phonons arises from the Jahn-Teller effect that splits the e_g double degeneracy (51). Then the Hamiltonian reads:

$$\begin{aligned} H = \quad & -t \sum_{i,\vec{\delta}} \left(\frac{S_0^{i,i+\vec{\delta}} + 1/2}{2S+1} \right) c_i^\dagger c_{i+\vec{\delta}} + \omega_0 \sum_i a_i^\dagger a_i \\ & + g\omega_0 \sum_i c_i^\dagger c_i \left(a_i + a_i^\dagger \right) \\ & + \frac{\epsilon}{2} \sum_{i,\vec{\delta}} \vec{S}_i \cdot \vec{S}_{i+\vec{\delta}} - \mu \sum_i c_i^\dagger c_i. \end{aligned} \tag{2.1}$$

Here t is the transfer integral of electrons occupying e_g orbitals between nearest neighbor (nn) sites, $S_0^{i,i+\vec{\delta}}$ is the total spin of the subsystem consisting of two localized spins on nn sites and the conduction electron, $\vec{S}_i$ is the spin of the t_{2g} core states ($S = 3/2$), $c_i^\dagger$ (c_i) creates (destroys) an electron with spin parallel to the ionic spin at the i-th site in the e_g orbital. The coordination vector $\vec{\delta}$ connects nn sites. The first term of the Hamiltonian describes the double-exchange mechanism in the limit where the intra-atomic exchange integral J is far larger than the transfer integral t. Furthermore in eq.(2.1) ω_0 denotes the frequency of the local optical phonon mode, $a_i^\dagger$ (a_i) is the creation (annihilation) phonon operator at the site i, the dimensionless parameter g indicates the strength of the electron-phonon interaction in the Holstein model (52), ϵ represents the antiferromagnetic super-exchange coupling between two nn t_{2g} spins and μ is the chemical potential. The hopping of electrons is supposed to take place between the equivalent nn sites of a simple cubic lattice separated by the distance $|n - n'| = a$. The units are such that the Planck constant $\hbar = 1$, the Boltzmann constant k_B=1 and

the lattice parameter a=1. In order to treat the electron-phonon interaction variationally, it has been used a scheme already proposed in a similar context (53) based on a modified Lang-Firsov canonical transformation and the Bogoliubov inequality (54; 55). The latter allows to fix an upper limit for the Free Energy F:

$$F \leq F_{test} + \langle \tilde{H} - H_{test} \rangle_t, \tag{2.2}$$

where F_{test} and H_{test} are the Free Energy and the Hamiltonian corresponding to the model that has been assumed as the ansatz. The symbol $<>_t$ indicates a thermodynamic average performed by using the test Hamiltonian.

Following ref.[(53)], it has been chosen H_{test} in such a way that electron, phonon and spin degrees of freedom are not interacting:

$$\begin{aligned} H_{test} = H^{el}_{test} + \omega_0 \sum_i a_i^\dagger a_i + \\ + N\omega_0 g^2 (1-x)^2 (1-f)^2 - g_s \mu_B \sum_i \vec{h}_{eff} \cdot \vec{S}_i. \end{aligned} \tag{2.3}$$

Here $N = N_x N_y N_z$ is total number of the lattice sites, g_s is the dimensionless electron spin factor ($g_s \simeq 2$), μ_B is the Bohr magneton. Furthermore, f and h_{eff} represent, respectively, the polaron localization parameter and the effective molecular magnetic field that are determined by the variational approach. In the test Hamiltonian (2.3), H^{el}_{test} reads

$$H^{el}_{test} = -te^{-S_T} \sum_{i,\vec{\delta}} \gamma_{\vec{\delta}} c_i^\dagger c_{i+\vec{\delta}} - \mu_{eff} \sum_i c_i^\dagger c_i, \tag{2.4}$$

where the factor e^{-S_T} controls the band renormalization due to the polaron formation and $\gamma_{\vec{\delta}}$ indicates the thermal average of the double-exchange spin operator

$$\gamma_{\vec{\delta}} = \left\langle \left(\frac{S_0^{i,i+\vec{\delta}} + 1/2}{2S+1} \right) \right\rangle_t, \tag{2.5}$$

that depends on relative orientation of the t_{2g} spin localized on (nn) sites. Furthermore, μ_{eff} represents the effective chemical potential. From the in-

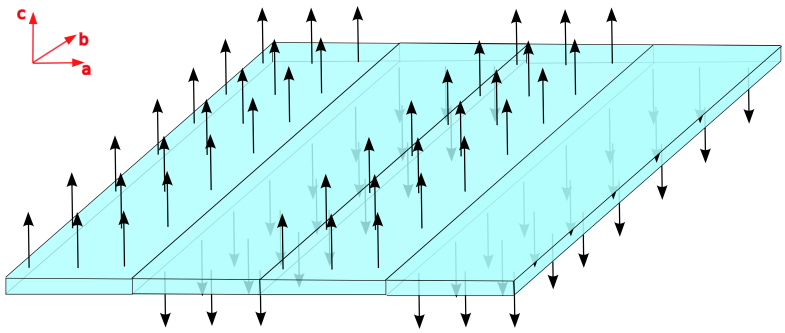

Figure 2.1: The picture schematically shows the magnetic-stripe order corresponding to in-plane anisotropic magnetic solutions.

equality (2.2) we obtain the variational free energy for single site:

$$\begin{aligned}\frac{F}{N} = \quad & f^{el}_{test} + T\log\left(1-e^{-\beta\omega_0}\right) + \omega_0 g^2(1-f)^2(1-x)^2 \\ & -T\log\nu_S + f^{ord}_{test} + T\lambda m_S,\end{aligned} \tag{2.6}$$

where f^{el}_{test} represents the electronic contribution to the free energy and f^{ord}_{test} depends on the magnetic order of the system. Both will be discussed in some details in the following. In Eq. (2.6) β is the inverse of the temperature, ν_S is the partition function of the localized spins, λ is a dimensionless variational parameter proportional to the effective magnetic field.

In order to calculate f^{el}_{test}, we need to know the energy spectrum of H_{test}. In particular we have to calculate the associated electronic eigenvalues. This calculation is carried out by diagonalizing the electronic contribution to the test hamiltonian. For MS solutions the derivation of the electron dispersion relation has to take into account the periodic nature of the solution. Actually, this solution introduces a positional dependence of the double-exchange factor that, in turn, modulates the effective transfer integral. In order to fix the ideas, the x-axis as the direction along which the MS alternate (a-direction) is assumed. Assuming that the transverse width of a single stripe is L, the corresponding dimension of the magnetic unit cell will be $(2L, 1, 1)$. (See the Fig. 1)

As mentioned above, the electronic part of H_{test} needs to be diagonalized

$$H^{el}_{test}|k_x k_y k_z, \alpha\rangle = \xi(k_x, k_y, k_z, \alpha)|k_x k_y k_z, \alpha\rangle. \tag{2.7}$$

Here k_x, k_y, k_z indicate the wave vectors of the magnetic lattice, α is the index of the magnetic unit cell and $\xi(k_x, k_y, k_z, \alpha)$ the electronic dispersion. In the ab plane, we employ periodic boundary conditions. On the other hand, the finite size of the film is taken into account considering the system made of a finite number of planes and imposing open boundary conditions along the out-of-plane direction of growth (56). The eigenvalue equation (2.7) with the boundary conditions mentioned above is equivalent to diagonalize the following matrix $2L \times 2L$

$$\begin{pmatrix} D(k_y,k_z) & F & \cdots & Ee^{-i2Lk_x} \\ F & D(k_y,k_z) & \cdots & 0 \\ \vdots & \vdots & \ddots & \vdots \\ Ee^{i2Lk_x} & 0 & \cdots & D(k_y,k_z) \end{pmatrix},$$

where

$$\begin{aligned} F &= -te^{-S_T}\gamma_{\delta_y} \\ E &= -te^{-S_T}\gamma_{\delta_x} \end{aligned} \tag{2.8}$$

represent the effective transfer integrals (2.5) for nearest-neighboring t_{2g} spin aligned and anti-aligned, respectively, while

$$D(k_y, k_z) = 2F\,(cos(k_y) + cos(k_z)) \tag{2.9}$$

represents the partial dispersion relation connected to directions where the t_{2g} spin are aligned. The electron free energy for a generic solution reads

$$f^{el}_{test} = -\frac{T}{(2\pi)^2 N_z}\sum_{k_z}\sum_{\alpha}\int_{-\frac{\pi}{2L}}^{\frac{\pi}{2L}} dk_x \int_{-\pi}^{\pi} dk_y \log\left(1 + e^{-\beta\xi(\mathbf{k},\alpha)}\right). \tag{2.10}$$

In eq.(2.10) N_z is the number of planes in the z direction.

The behavior of the MS solutions with different transverse widths L have been analyzed. In particular, $L = 1$ has been compared with $L = 2$ and $L = 3$ (this last case is sketched in Fig.1). In every case, in the magnetic super-cell, we stress that there is only one anti-ferromagnetic bond along the x-axis. The solutions differ each other for the number of the ferromagnetic bonds: 0 for $L = 1$, 2 for $L = 2$, 4 for $L = 3$. In the parameter range where the anti-ferromagnetic solutions are favored (smaller t), the solution with $L = 1$ becomes more stable in comparison with MS phases characterised by larger values of L. On the contrary, in the parameter range where ferromagnetic solutions are favoured (larger t), phases with larger value of L have lower energies with respect to the case $L = 1$. However, in this case, the phases with L larger than 1 have always energies higher than those of the homogeneous ferromagnetic phase by varying the parameters hopping t, temperature T and number of planes N_z in the z direction. Therefore, the most stable solution, among the MS ones, corresponds to that with the minimal transverse width of the stripes ($L = 1$). For this magnetic order we can exhibit the electronic band in a closed form:

$$\xi_{\mathbf{k}} = Ecos(k_x) + Fcos(k_y) + Fcos(k_z) - \mu_{eff}. \tag{2.11}$$

For $L = 1$ we obtain also a simple compact form for f_{test}^{ord}:

$$f_{test}^{ord} = \left(\pm 3 - \frac{1}{N_z}\right) \varepsilon S^2 m_S^2, \tag{2.12}$$

where the top and bottom signs hold, respectively, for the ferromagnetic and antiferromagnetic solutions. While for magnetic-stripe solution this becomes

$$f_{test}^{ord} = \left(1 - \frac{1}{N_z}\right) \varepsilon S^2 m_S^2. \tag{2.13}$$

In the present study an important role is played by the hopping amplitude. Actually, the change of the hopping amplitude is able to trigger the stabilization of the MS phase. It is well known that there is a close connection between t and the biaxial strain due to the substrate. It has been carefully shown (7; 8) that in epitaxial thin film of $La_{1-x}Ca_xMnO_3$, grown on

substrates with significant tensile lattice mismatch, the in-plane parameter increases while the out-of-plane lattice constant is reduced. Similar results are also reported in Ref.(9), where the out-of-plane lattice parameter, c, in $LSMO$ epitaxial thin film was measured as a function of the film thickness showing a reduction of c for thinner films. These results suggest that when the film's thickness is smaller than $400\mathring{A}$ some tensile strain is present in the ab plane. Consequently, the in-plane parameter increases and the hopping amplitude decreases. Summarizing, the conjecture is that the reduction of the thickness *drives* a reduction of the transfer integral.

In Fig.(2.2) the hopping amplitude-temperature phase diagram, for the case of $N_z = 2$ is showed. It is clear that the anisotropic phase with $(L = 1)$ stabilizes in a wide region between antiferro-magnetic and ferro-magnetic phases. The existence of the MS phase can be understood as a reasonable compromise between the two homogeneous phases that at their interface exhibit a higher energy. Furthermore, the phase separation between magnetically ordered and paramagnetic phase is not modified by the presence of the MS phase suggesting that the MI transition (driven by the FM-PM transition) is not modified by the stabilisation of the MS phase. It is also notable the *re-entrant* shape of the stability region for the MS phase, that determines, for suitable values of hopping amplitude t, an interesting sequence of order-order transition: FM$\mapsto$MS and MS$\mapsto$FM. Finally, I would emphasize that the numerical results, for the set of parameters used in this work and suitable for LSMO (9), provide itinerant wave-functions for the electrons. The mass renormalization, due to the electron-phonon coupling, is not very large and we do not see any polaron self-trapping in the magnetically ordered phases.

Moreover the stability of the MS phase [see Fig.(2.3)] for different numbers of planes has been studied and it has been found that the MS phase moves slightly towards larger t values when the number of layers increases, saturating around 100 layers. We also observe that, at very low temperatures, the range of hopping, where the MS solution stabilizes, decreases as the number of layers increases.

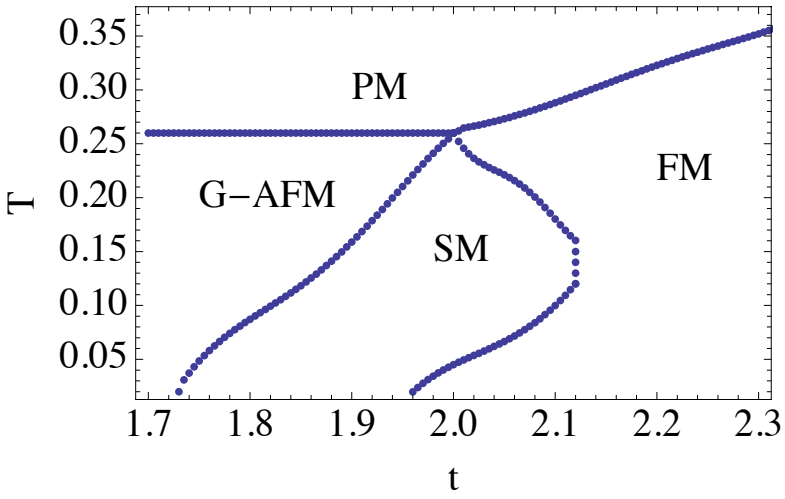

Figure 2.2: Phase diagram in the hopping-temperature plane for $N_z = 2$ at fixed hole density ($x = 0.3$), correspondig to $g = 2$ and $\varepsilon = 0.05\omega_0$. PM means paramagnetic metal, FM ferromagnetic metal, G-AFM G-type antiferromagnetic metal and finally MS indicates the magnetic-stripe solution. The transfer integral t and the temperature T are expressed in units of ω_0.

It is worth noticing that, starting from a value of the hopping amplitude corresponding to the region where FM stabilizes, the MS phase stabilizes reducing the hopping amplitude. In the numerical results the extent of reduction of hopping amplitude that leads to transition FM↦MS is compatible to the typical extent of in-plane lattice parameter caused by tensile strain. I end this section with a general remark on the anisotropy observed in thin films of LSMO grown on different substrates. As matter of the fact, for suitable values of hopping, where the MS stabilizes, we have shown that an anisotropic behavior in the in-plane properties of the film takes in. How can this be linked to the experimental data? As already mentioned, for epitaxial thin film coherently strained by in-plane tensile strain, for thickness such that the mismatch causes an increase of the in-plane lattice parameter we expect a decrease of the effective hopping amplitude. Actually, even for moderate compressive strain, a decrease of the c-axis has been observed in those very thin films exhibiting anisotropic behavior. This sugges that, also in this case,

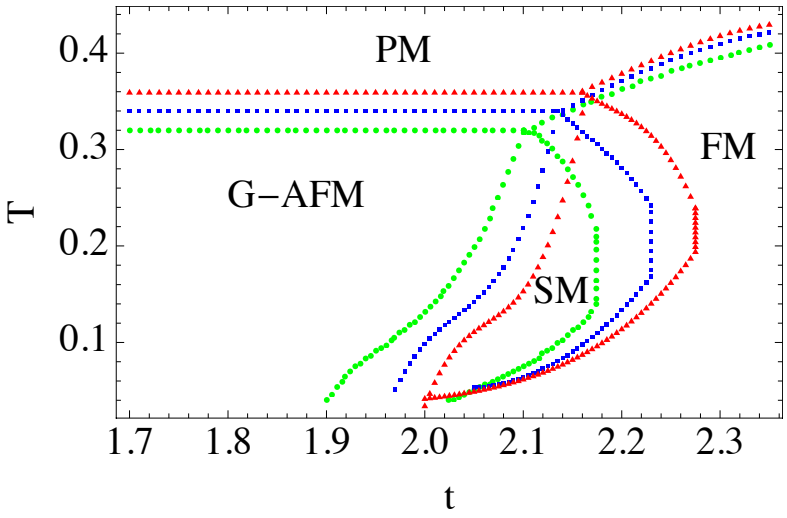

Figure 2.3: Comparison among the phase diagrams corresponding to different thicknesses: $N_z = 5$ (full circles, green), $N_z = 10$ (full squares, blue) and $N_z = 100$ (full triangles, red). PM means paramagnetic metal, FM ferromagnetic metal, G-AFM G-type antiferromagnetic metal and finally MS indicates the magnetic-stripe solution. The transfer integral t and the temperature T are expressed in units of ω_0.

the effective hopping amplitude could decrease.

2.2 Resistivity: in-plane anisotropy

In order to show that the stabilisation of the MS phase can, indeed, lead to the anisotropy observed experimentally, in this section, the resistivity for temperatures lower than FM↦PM transition has been calculated.

It is well known that the resistivity is given by the inverse of the $\omega \mapsto 0$ limit of the real part of $\sigma_{\alpha,\alpha}(\omega)$ that is related to the current-current correlation function, $\Pi^{ret}_{\alpha,\alpha}(\omega)$, by

$$\Re\sigma_{\alpha,\alpha}(\omega) = -\frac{\Im\Pi^{ret}_{\alpha,\alpha}(\omega)}{\omega}. \tag{2.14}$$

Therefore our problem reduces to evaluate the current-current correlation function. Following the scheme introduced in Ref.[(53)] and limiting our analysis only to the coherent contribution of the conductivity, it is possible to show that, in Matsubara frequencies, $\Pi^{coh}_{\alpha,\alpha}(i\omega_n)$ becomes

$$\Pi^{coh}_{\alpha,\alpha}(i\omega_n) = 4e^2t^2e^{-2S_T}\left(\frac{1}{(2\pi)^2N_z}\right)\gamma^2_{\delta_\alpha}$$
$$\sum_{k_z}\int_{-\pi}^{\pi}dk_x\int_{-\pi}^{\pi}dk_y\sin^2(k_\alpha)\int_0^\beta e^{i\omega_n\tau}\tilde{\mathcal{G}}(\mathbf{k},-\tau)\tilde{\mathcal{G}}(\mathbf{k},\tau), \tag{2.15}$$

where the index α refers to one of the two in-plane directions. In this approach Π depends on γ_{δ_α} defined in eq.(2.5). The restriction to coherent processes for the current-current correlation function is justified at low temperatures where the multi-phonon in-coherent contribution is expect not to play a main role. We remember that, below the FM↦PM critical temperature, our variational analysis does not support the existence of phonon induced localization for the charge carriers that is, usually, associated to the incoherent transport. On the contrary the charge electrons have an itinerant nature both in FM and MS phases. The situation changes in the high temperature paramagnetic phase where the formation of small polarons are

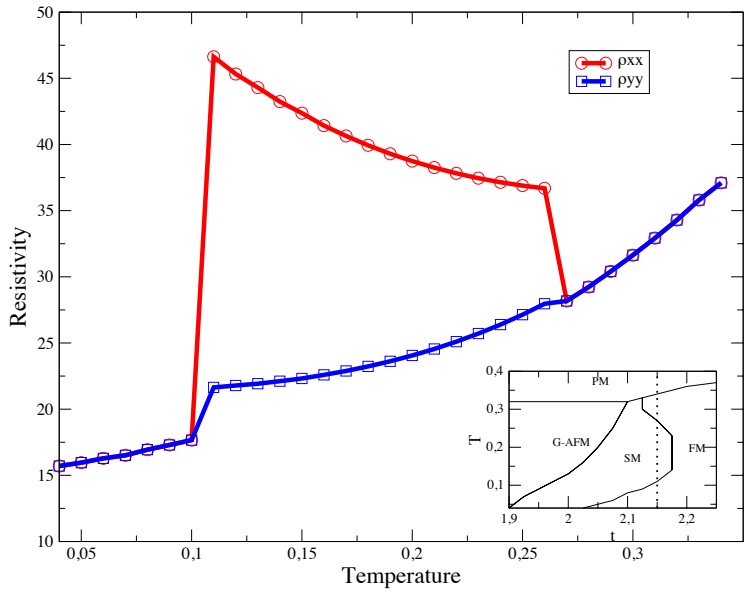

Figure 2.4: Resistivity vs temperature in the ab-plane for a 5-layer thick film: ρ_{xx} (full line, red) and ρ_{yy} (dashed line, green) corresponding to $g = 2$ and $\varepsilon = 0.05\omega_0$ for a fixed value of hopping amplitude $t = 2.15\omega_0$. The resistivity is expressed in unit of $\frac{e^2}{a\hbar}$ and T in units of ω_0. In the inset the phase diagram $(T - t)$, corresponding to 5 layers, is shown.

favoured giving rise to an insulating phase due to the cooperative effect of disorder.

Making the analytic continuation $i\omega_n \to \omega + i\delta$ in (2.15) and by using eq. (2.14), it is possible to get the conductivity tensor and, hence, the in-plane resistivity, both along the stripes and perpendicular to them. However, in order to calculate the current-current correlation function [eq.(2.15)] we still need a reasonable approximation for $\tilde{\mathcal{G}}$. Following again Ref.[(53)], the Green function can be carried out using the Lehmann representation

$$\tilde{\mathcal{G}}(\mathbf{k}, i\omega_n) = \int_{-\infty}^{+\infty} \frac{d\omega}{2\pi} \frac{\tilde{A}(\mathbf{k}, \omega)}{i\omega_n - \omega} \tag{2.16}$$

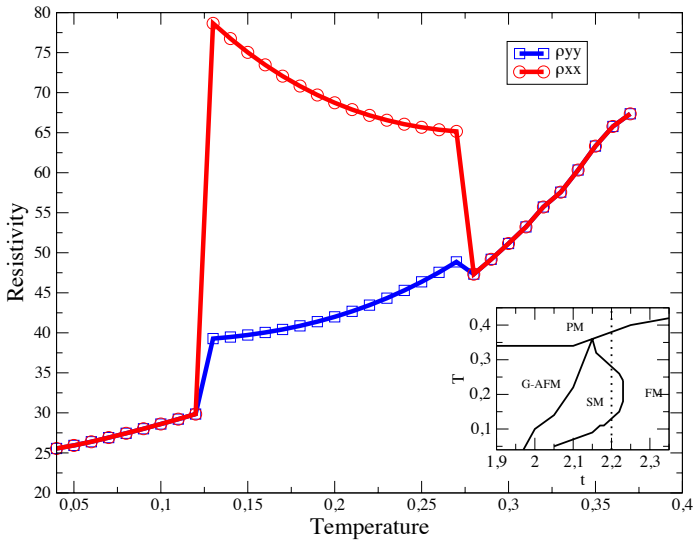

Figure 2.5: Resistivity vs temperature in the ab-plane for a 10-layer thick film: ρ_{xx} (full line, red) and ρ_{yy} (dashed line, green) corresponding to $g = 2$ and $\varepsilon = 0.05\omega_0$ for a fixed value of hopping amplitude $t = 2.2\omega_0$. The resistivity is expressed in unit of $\frac{e^2}{a\hbar}$ and T in units of ω_0. In the inset the phase diagram $(T - t)$, corresponding to 10 layers, is shown.

and assuming for the spectral function $\tilde{A}$

$$\tilde{A}(\mathbf{k},\omega) = \frac{\Gamma(\mathbf{k})}{[\Gamma(\mathbf{k})]^2/4 + (\omega - \xi_{\mathbf{k}})^2,} \tag{2.17}$$

with $\Gamma(\mathbf{k})$ corresponding to the itinerant polaron scattering rate. Due to the finite size along z-axis, the contribution of the single-phonon (55) to the scattering rate $\Gamma(\mathbf{k})$ reads

$$\Gamma_{1-phon}(\mathbf{k}) = \sum_{k_z'} \Big[t^2 e^{-2S_T} C^{ord}(k_z, k_z') I_1(s) \sinh\left(\frac{\beta\omega_0}{2}\right) + g^2\omega_0^2(1-f)^2 \Big] h(\mathbf{k}, k_z'). \tag{2.18}$$

In eq.(2.18) the dependence on magnetic solution is contained in the factor

$$C^{ord}(k_z, k_z') = 4(\gamma_{\delta_x}^2 + \gamma_{\delta_y}^2 + \gamma_{\delta_z}^2)\Phi_1(k_z, k_z') + (4\gamma_{\delta_x}^2 + 4\gamma_{\delta_y}^2 + 2\gamma_{\delta_z}^2)\Phi_2(k_z, k_z'), \tag{2.19}$$

where $\Phi_1(k_z, k_z')$ and $\Phi_2(k_z, k_z')$ are given by

$$\Phi_1(k_z, k_z') = \sum_{l=2}^{N_z-1} \phi^2(lk_z)\phi^2(lk_z')$$
$$\Phi_2(k_z, k_z') = \phi^2(k_z)\phi^2(k_z') + \phi^2(N_z k_z)\phi^2(N_z k_z') \tag{2.20}$$

and $\phi(lk_z)$ represents the projection of the electron eigen-states of the test hamiltonian along the z-axis (56). Moreover $h(\mathbf{k}, k_z')$ is given by

$$h(\mathbf{k}, k_z') = 2\pi e^{-S_T} g(k_z')$$
$$[1 + 2n_B(\omega_0) + n_F(\omega_0 + \xi_{\mathbf{k}}) - n_F(\xi_{\mathbf{k}} - \omega_0)], \tag{2.21}$$

where n_B and n_F indicate boson and fermion average occupation numbers, respectively. Furthermore $g(k_z')$ is the constant density of states for fixed k_z', while $I_1(s)$ is the modified Bessel function calculated for $s = 2f^2g^2[n_B(\omega_0)(n_B(\omega_0)+$

$1)]^{1/2}$. It is worth noting that the single phonon scattering approximation has been already successfully used in the case of manganite films and bulk (56). The reason why we can do this is that we have treated the residual electron-phonon interaction at the lowest order, after considering the interaction itself at the variational Lang-Firsov level.

In the figures (2.4) and (2.5) we show the resistivity obtained by our approach. Clearly the resistivity exhibits a strong anisotropy depending if the current is flowing along the stripes or perpendicular to them. The resistivity anisotropy is tightly related to the magnetic transition FM$\mapsto$MS.

Along the stripes the core spins are all aligned, both in the FM and MS phases, and the resistivity shows a metallic behavior very similar to the one expected in the homogenous FM phase and observed in thicker films and bulk samples. On the other hand, along the direction perpendicular to the MS, where the spins are aligned in the FM phase and anti-aligned in MS phase, the resistivity jumps at the temperatures corresponding to the FM $\mapsto$ MS and MS $\mapsto$ FM transitions, respectively. The jumps are related to the different role played by the double exchange in the FM and MS phases. In the latter the antiferromagnetic order reduces the double exchange effective transfer integral reducing the mobility of the e_g electrons as it is evident from eq.(2.8). It should be noticed here that the abrupt jump could be related to the fact that disorder effects are not included in our analysis. Actually, disorder effects are able to smooth first-order transitions. In this case, therefore, disorder should be able to affect the transition between the ferromagnetic and MS phase. In any case, it is important to observe that the size of the jump (around a factor 2) is in a good agreement with the value reported in the experiments. The reduction of the mobility of the e_g electrons in the MS phase finds confirm, also, in the insulating behavior exhibited by the resistivity along the direction perpendicular to the stripes between the two jumps. This behavior can be explained by the dependence on temperature of the double-exchange spin factor (2.5) for anti-aligned (nn) t_{2g} spin. Indeed, the latter increases as the temperature increases improving

the mobility of the e_g electrons. For this reason the resistivity along such direction decreases into the range where MS solution stabilizes. Finally, into the range of temperatures where ferromagnetic solution stabilizes again, the in-plane components of the resistivity tensor, along the MS and perpendicular to them, coincide and resume to increase with temperature.

Chapter 3

Manganite heterostructures: the case of a single interface

In this chapter a correlated inhomogeneous mean-field approach is proposed in order to study a tight-binding model of the manganite heterostructures $(LaMnO_3)_{2n}/(SrMnO_3)_n$ with average hole doping $x = 1/3$. Phase diagrams, spectral and optical properties of large heterostructures (up to 48 sites along the growth direction) with a single interface are discussed analyzing the effects of electron-lattice anti-adiabatic fluctuations and strain. The formation of a metallic ferromagnetic interface is quite robust with varying the strength of electron-lattice coupling and strain, though the size of the interface region is strongly dependent on these interactions. The density of states never vanishes at the chemical potential due to the formation of the interface, but it shows a rapid suppression with increasing the electron-lattice coupling. The in-plane and out-of-plane optical conductivities show sharp differences since the in-plane response has metallic features, while the out-of-plane one is characterized by a transfer of spectral weight to high frequency. The in-plane response mainly comes from the region between the two insulating blocks, so that it provides a clear signature of the formation of the metallic ferromagnetic interface.

3.1 The variational approach

3.1.1 Model Hamiltonian

For manganite superlattices, the hamiltonian of the bulk H_0 has to be supplemented by Coulomb terms representing the potential arising from the pattern of the La and Sr ions, (**?**) thus

$$H = H_0 + H_{Coul}. \tag{3.1}$$

In order to set up an appropriate model for the double layer, it is important to take into account the effects of the strain. The epitaxial strain produces the tetragonal distortion of the MnO_6 octahedron, splitting the e_g states into $x^2 - y^2$ and $3z^2 - r^2$ states. (**?**) If the strain is tensile, $x^2 - y^2$ is lower in energy, while, if the strain is compressive, $3z^2 - r^2$ is favored. In the case of $n = 8$ and three interfaces, (15) the superlattices grown on STO are found to be coherently strained: all of them are forced to the in-plane lattice parameter of substrate and to an average out-of-plane parameter $c \simeq 3.87\mathring{A}$. (15) As a consequence, one can infer that LMO blocks are subjected to compressive strain (-2.2%) and SMO blocks to tensile strain ($+2.6\%$). For the case of LMO block, the resulting higher occupancy of $3z^2 - r^2$ enhances the out-of-plane ferromagnetic interaction owing to the larger electron hopping out-of-plane. For the case of SMO block, the reverse occurs. A suitable model for the bilayer has to describe the dynamics of the e_g electrons which in LMO block and SMO block preferentially occupy the more anisotropic $3z^2 - r^2$ orbitals and more isotropic $x^2 - y^2$ orbitals, respectively. For this reason, in this paper we adopt an effective single orbital approximation for the bulk manganite.

The model for the bulk takes into account the double-exchange mechanism, the coupling to the lattice distortions and the super-exchange interaction between neighboring localized t_{2g} electrons on Mn ions. The coupling to longitudinal optical phonons arises from the Jahn-Teller effect that splits the e_g double degeneracy. Then, the Hamiltonian H_0 reads:

$$
\begin{aligned}
H_0 = \quad & -\sum_{\vec{R}_i,\vec{\delta}} t_{|\vec{\delta}|}\left(\frac{S_0^{\vec{R}_i,\vec{R}_i+\vec{\delta}}+1/2}{2S+1}\right) c^{\dagger}_{\vec{R}_i} c_{\vec{R}_i+\vec{\delta}} \\
& +\omega_0 \sum_{\vec{R}_i} a^{\dagger}_{\vec{R}_i} a_{\vec{R}_i} + g\omega_0 \sum_{\vec{R}_i} c^{\dagger}_{\vec{R}_i} c_{\vec{R}_i}\left(a_{\vec{R}_i}+a^{\dagger}_{\vec{R}_i}\right) \\
& +\frac{1}{2}\sum_{\vec{R}_i,\vec{\delta}} \epsilon_{|\vec{\delta}|}\vec{S}_{\vec{R}_i}\cdot\vec{S}_{\vec{R}_i+\vec{\delta}} - \mu\sum_{\vec{R}_i} c^{\dagger}_{\vec{R}_i} c_{\vec{R}_i}. \qquad (3.2)
\end{aligned}
$$

Here $t_{|\vec{\delta}|}$ is the transfer integral of electrons occupying e_g orbitals between nearest neighbor (nn) sites, $S_0^{\vec{R}_i,\vec{R}_i+\vec{\delta}}$ is the total spin of the subsystem consisting of two localized spins on nn sites and the conduction electron, $\vec{S}_{\vec{R}_i}$ is the spin of the t_{2g} core states ($S=3/2$), $c^{\dagger}_{\vec{R}_i}\left(c_{\vec{R}_i}\right)$ creates (destroys) an electron with spin parallel to the ionic spin at the i-th site in the e_g orbital. The coordination vector $\vec{\delta}$ connects nn sites. The first term of the Hamiltonian describes the double-exchange mechanism in the limit where the intra-atomic exchange integral J is far larger than the transfer integral $t_{|\vec{\delta}|}$. Furthermore, in eq.(3.2), ω_0 denotes the frequency of the local optical phonon mode, $a^{\dagger}_{\vec{R}_i}\left(a_{\vec{R}_i}\right)$ is the creation (annihilation) phonon operator at the site i, the dimensionless parameter g indicates the strength of the electron-phonon interaction. Finally, in Eq.(3.2), $\epsilon_{|\vec{\delta}|}$ represents the antiferromagnetic super-exchange coupling between two nn t_{2g} spins and μ is the chemical potential. The hopping of electrons is supposed to take place between the equivalent nn sites of a simple cubic lattice (with finite size along the z axis corresponding to the growth direction of the heterostructure) separated by the distance $|n-n'|=a$. The units are such that the Planck constant $\hbar=1$, the Boltzmann constant k_B=1 and the lattice parameter a=1.

Regarding the terms due to the interfaces, one considers that La^{3+} and Sr^{2+} ions act as +1 charges of magnitude e and neutral points, respectively. In the heterostructure, the distribution of those cations induces an interaction term for e_g electrons of Mn giving rise to the Hamiltonian

$$H_{Coul} = \sum_{\vec{R}_i \neq \vec{R}_j} \frac{1}{2\epsilon_d} \frac{e^2 n_{\vec{R}_i} n_{\vec{R}_j}}{|\vec{R}_i - \vec{R}_j|} + \sum_{\vec{R}_i^{La} \neq \vec{R}_j^{La}} \frac{1}{2\epsilon_d} \frac{e^2}{|\vec{R}_i^{La} - \vec{R}_j^{La}|} - \sum_{\vec{R}_i, \vec{R}_j^{La}} \frac{1}{\epsilon_d} \frac{e^2 n_{\vec{R}_i}}{|\vec{R}_i - \vec{R}_j^{La}|}, \tag{3.3}$$

with $n_{\vec{R}_i} = c^{\dagger}_{\vec{R}_i} c_{\vec{R}_i}$ electron occupation number at Mn site i, $\vec{R}_i$ and $\vec{R}_i^{La}$ are the positions of Mn and La^{3+} in ith unit cell, respectively, and ϵ_d is the dielectric constant of the material. In this calculation the long-range Coulomb potential has been modulated by a factor η inducing a fictitious finite screening-length. This factor was added only for computational reasons since it allows to calculate the summations of the Coulomb terms over the lattice indices. The heterostructures have been modulated by slabs whose in-plane size is infinite.

In order to describe the magnitude of the Coulomb interaction, it has been defined the dimensionless parameter $\alpha = e^2/(a\epsilon_d t_{|\vec{\delta}|})$ which controls the charge-density distribution. The order of magnitude of α can be estimated from the hopping parameter $t_{|\vec{\delta}|} \sim 0.65eV$, lattice constant $a = 4\mathring{A}$, and typical value of dielectric constant $\epsilon \sim 10$ to be around 0.2.

Strain plays an important role also by renormalizing the heterostructure parameters. Strain effects can be simulated by introducing an anisotropy into the model between the in-plane hopping amplitude $t_{\delta_{||}} = t$ (with $\delta_{||}$ indicating nearest neighbors in the $x - y$ planes) and out-of-plane hopping amplitude $t_{|\delta_z|} = t_z$ (with δ_z indicating nearest neighbors along z axis). (57) Moreover, the strain induced by the substrate can directly affect the patterns of core spins. (32) Therefore, in the used model, it has also been considered the anisotropy between the in-plane super-exchange energy $\epsilon_{|\delta_{||}|} = \epsilon$ and the out-of-plane one $\epsilon_{|\delta_z|} = \epsilon_z$. We have found that the stability of magnetic phases in LMO blocks is influenced by the the presence of compressive strain, while in SMO the sensitivity to strain is poor. Therefore, in all the treating, it has been taken as reference the model parameters of the SMO layers and

it will be considered anisotropy only in the LMO blocks with values of the ratio t_z/t larger than unity and of the ratio ϵ_z/ϵ smaller than unity.

Finally, in order to investigate the effects of the electron-lattice coupling, it will be used the dimensionless quantity λ defined as

$$\lambda = \frac{g^2\omega_0}{6t}. \tag{3.4}$$

In all the paper we will assume $\omega_0/t = 0.5$.

3.1.2 Test Hamiltonian

In this work, it will be considered solutions of the hamiltonian that break the translational invariance in the out-of-plane z-direction. The thickness of the slab is a parameter of the system that will be indicated by N_z. It will be build up a variational procedure including these features of the heterostructures. A simplified variational approach similar to that developed in this work has already been proposed by some of the authors for manganite bulks (58) and films. (59; 17)

In order to treat variationally the electron-phonon interaction, the Hamiltonian (3.1) has been subjected to an inhomogeneous Lang-Firsov canonical transformation. (60) It is defined by parameters depending on plane indices along z-direction:

$$U = exp\left[-g\sum_{i_{||},i_z}(f_{i_z}c^{\dagger}_{i_{||},i_z}c_{i_{||},i_z} + \Delta_{i_z})(a_{i_{||},i_z} - a^{\dagger}_{i_{||},i_z})\right], \tag{3.5}$$

where $i_{||}$ indicates the in-plane lattice sites (i_x, i_y), while i_z the sites along the direction z. The quantity f_{i_z} represents the strength of the coupling between an electron and the phonon displacement on the same site belonging to i_z-plane, hence it measures the degree of the polaronic effect. On the other hand, the parameter Δ_{i_z} denotes a displacement field describing static distortions that are not influenced by instantaneous position of the electrons.

In order to obtain an upper limit for free energy, the Bogoliubov inequality has been adopted:

$$F \leq F_{test} + \langle \tilde{H} - H_{test} \rangle_t, \tag{3.6}$$

where F_{test} and H_{test} are the free energy and the Hamiltonian corresponding to the test model that is assumed with an ansatz. $\tilde{H}$ stands for the transformed Hamiltonian $\tilde{H} = UHU^\dagger$. The symbol $\langle\rangle_t$ indicates a thermodynamic average performed by using the test Hamiltonian. The only part of H_{test} which contributes to $\langle \tilde{H} - H_{test} \rangle_t$ is given by the spin freedom degrees and depends on the magnetic order of the t_{2g} core spins. For the spins, this procedure is equivalent to the standard mean-field approach.

The model test hamiltonian, H_{test}, is such that that electron, phonon and spin degrees of freedom are not interacting with each other:

$$H_{test} = H^{sp}_{test} + H^{ph}_{test} + H^{el}_{test}. \tag{3.7}$$

The phonon part of H_{test} simply reads

$$H^{ph}_{test} = \omega_0 \sum_{i_{||}, i_z} a^\dagger_{i_{||}, i_{i_z}} a_{i_{||}, i_{i_z}}, \tag{3.8}$$

and the spin term is given by

$$H^{sp}_{test} = -g_S \mu_B \sum_{i_{||}} \sum_{i_z} h^z_{i_{||}, i_z} S^z_{i_{||}, i_z}, \tag{3.9}$$

where g_S is the dimensionless electron-spin factor ($g_S \simeq 2$), μ_B is the Bohr magneton, and $h^z_{i_{||}, i_z}$ is the effective variational magnetic field. In this work, we consider the following magnetic orders modulated plane by plane:

$$\begin{aligned}
&F, \qquad h^z_{i_{||}, i_z} = |h^z_{i_z}|; \\
&A, \qquad h^z_{i_{||}, i_z} = (-1)^{i_z} |h^z_{i_z}|; \\
&C, \qquad h^z_{i_{||}, i_z} = (-1)^{ix+iy} |h^z_{i_z}|; \\
&G, \qquad h^z_{i_{||}, i_z} = (-1)^{ix+iy+iz} |h^z_{i_z}|.
\end{aligned} \tag{3.10}$$

For all these magnetic orders, the thermal averages of double-exchange operator, corresponding to neighboring sites in the same plane i_z $\gamma_{i_z; i_{||}, i_{||}+\delta_{||}}$ and

in different planes $\eta_{i_z,i_z+\delta_z;i_{||}}$, preserve only the dependence on the z plane index:

$$\gamma_{i_z;i_{||},i_{||}+\delta_{||}} = \langle \frac{S_0^{i_{||},i_z;i_{||}+\delta_{||},i_z} + 1/2}{2S+1} \rangle_t = \gamma_{i_z}$$
$$\eta_{i_z,i_z+\delta_z;i_{||}} = \langle \frac{S_0^{i_{||},i_z;i_{||},i_z+\delta_z} + 1/2}{2S+1} \rangle_t = \eta_{i_z,i_z+\delta_z}. \tag{3.11}$$

In order to get the mean-field electronic Hamiltonian, we make the Hartree approximation for the Coulomb interaction. The electronic contribution H^{el}_{test} to the test Hamiltonian becomes

$$\begin{aligned} H^{el}_{test} \quad &= -t \sum_{i_{||}} \sum_{i_z=1}^{N_z} \sum_{\delta_{||}} \gamma_{i_z} e^{-V_{i_z}} c^{\dagger}_{i_{||},i_z} c_{i_{||}+\delta_{||},i_z} \\ &-t_z \sum_{i_{||}} \sum_{i_z=1}^{N_z} \sum_{\delta_z} \eta_{i_z,i_z+\delta_z} e^{-W_{i_z,i_z+\delta_z}} c^{\dagger}_{i_{||},i_z} c_{i_{||},i_z+\delta_z} \\ &+ \sum_{i_{||}} \sum_{i_z=1}^{N_z} \left[\phi_{eff}(i_z) - \mu\right] c^{\dagger}_{i_{||},i_z} c_{i_{||},i_z} \\ &+N_x N_y (T_1 + T_2) + N_x N_y g^2 \omega_0 \sum_{i_z} \Delta_{i_z}. \end{aligned} \tag{3.12}$$

In Eq.(3.12), the quantity $\phi_{eff}(i_z)$ indicates the effective potential seen by the electrons. It consists of the Hartee self-consistent potential $\phi(i_z)$ (see Appendix A) and a potential due to the electron-phonon coupling:

$$\phi_{eff}(i_z) = \phi(i_z) + g^2 \omega_0 C_{i_z}, \tag{3.13}$$

with

$$C_{i_z} = f_{i_z}^2 - 2f_{i_z} + 2\Delta_{i_z}(f_{i_z} - 1). \tag{3.14}$$

The factors $e^{-V_{i_z}}$ and $e^{-W_{i_z,i_z+\delta_z}}$ represent the phonon thermal average of Lang-Firsov operators:

$$e^{-V_{i_z}} = \langle X_{i_{||},i_z} X^{\dagger}_{i_{||}+\delta_{||},i_z} \rangle_t$$
$$e^{-W_{i_z,i_z+\delta_z}} = \langle X_{i_{||},i_z} X^{\dagger}_{i_{||},i_z+\delta_z} \rangle_t, \tag{3.15}$$

where the operator $X_{\vec{R}_i}$ reads

$$X_{\vec{R}_i} = e^{gf_{i_z}(a_{\vec{R}_i} - a^{\dagger}_{\vec{R}_i})}.$$

Finally, the quantity T_1 and T_2 derive from the Hartree approximation (see Appendix A), N_x and N_y denote the size of the system along the two in-plane directions, respectively. In order to calculate the variational free energy, we need to know eigenvalues and eigenvectors of H^{el}_{test} which depend on the magnetic order of core spins through the double exchange terms.

3.1.3 Effective electronic Hamiltonian: the inclusion of the Hartree approximation

In this section we give some details about the effective electronic Hamiltonian derived within our approach. After the Hartree approximation for the long-range Coulomnb interactions, the mean-field electronic Hamiltonian reads:

$$\begin{aligned} H^{el}_{test} = & -t\sum_{i_{||}}\sum_{i_z=1}^{N_z}\sum_{\delta_{||}}\gamma_{i_z}e^{-V_{i_z}}c^{\dagger}_{i_{||},i_z}c_{i_{||}+\delta_{||},i_z} \\ & -t\sum_{i_{||}}\sum_{i_z=1}^{N_z}\sum_{\delta_z}\eta_{i_z,i_z+\delta_z}e^{-W_{i_z,i_z+\delta_z}}c^{\dagger}_{i_{||},i_z}c_{i_{||},i_z+\delta_z} \\ & +\sum_{i_{||}}\sum_{i_z=1}^{N_z}[\phi(i_z)-\mu]c^{\dagger}_{i_{||},i_z}c_{i_{||},i_z} + N_xN_y(T_1+T_2) \\ & +N_xN_yg^2\omega_0\sum_{i_z}\Delta_{i_z} + \sum_{i_{||}}\sum_{i_z=1}^{N_z}C_{i_z}(g^2\omega_0)c^{\dagger}_{i_{||},i_z}c_{i_{||},i_z}. \end{aligned} \tag{3.16}$$

The self-consistent Hartee potential is given by

$$\begin{aligned} \phi(i_z) = & \frac{e^2}{\epsilon}[\sum_{j_z>i_z}\chi(j_z)S(i_z-j_z) + \\ & \sum_{j_z<i_z}\chi(j_z)S(i_z-j_z) + S_1(0)\chi(i_z) - S_2(i_z)], \end{aligned} \tag{3.17}$$

where the quantity T_1 is

$$T_1 = \frac{-e^2}{2\epsilon}[\sum_{i_z=1}^{N_z}\sum_{j_z>i_z}^{N_z}\chi_{i_z}\chi_{j_z}S(i_z-j_z)+ \sum_{j_z<i_z}^{N_z}\chi_{i_z}\chi_{j_z}S(i_z-j_z)+S_1(0)\sum_{i_z}^{N_z}\chi_{i_z}^2], \tag{3.18}$$

and T_2

$$T_2 = \frac{e^2}{2\epsilon}[\sum_{I_z=1}^{N_{La}}\sum_{J_z>I_z}^{N_{La}}S(I_z-J_z)+ \sum_{J_z<I_z}^{N_{La}}S(I_z-J_z)+N_{La}S_1] \tag{3.19}$$

with $S(n_z)$, $S_1(0)$ end $S_2(n_z)$ obtained by adding the Coulomb terms on in-plane lattice index. The summations have been made modulating the Coulomb interaction with a screening factor: $\frac{e^2}{|\vec{r}_i-\vec{r}_j|} \rightarrow \frac{e^2e^{-\eta_S|\vec{r}_i-\vec{r}_j|}}{|\vec{r}_i-\vec{r}_j|}$, where $\frac{1}{\eta_S}$ is a fictitious finite screening length in units of the lattice parameter a. Therefore, $S(n_z)$ is

$$S(n_z) = \sum_{m_x,m_y}\frac{\exp\left(-\eta_S\sqrt{m_x^2+m_y^2+n_z^2}\right)}{\sqrt{m_x^2+m_y^2+n_z^2}}, \tag{3.20}$$

$S_1(0)$ is given by

$$S_1(0) = \sum_{m_x,m_y}\frac{\exp\left(-\eta_S\sqrt{m_x^2+m_y^2}\right)}{\sqrt{m_x^2+m_y^2}}, \tag{3.21}$$

with $(m_x, m_y) \neq (0,0)$, and $S_2(i_z-j_z)$ is

$$S_2(n_z) = \sum_{m_x,m_y}\sum_{i_z=1}^{l_z}\frac{\exp\left(-\eta_S\sqrt{h_x^2+h_y^2+h_z^2}\right)}{\sqrt{h_x^2+h_y^2+h_z^2}}, \tag{3.22}$$

with l_z number of the planes of LMO block, $h_x = m_x - 0.5$, $h_y = m_y - 0.5$, and $h_z = n_z - i_z - 0.5$.

3.1.4 Magnetic order and diagonalization of the electronic mean-field Hamiltonian

In order to develop the calculation, we need to fix the magnetic order of core spins. The patters of magnetic orders is determined by the minimization of the total free energy. By exploiting the translational invariance along the directions perpendicular to the growth axis of the heterostructure, the diagonalization for H^{el}_{test} reduces to an effective unidimensional problem for each pair of continuous wave vectors $(k_x, k_y) = \vec{k}_{||}$. For some magnetic patterns, the electronic problem is characterized at the interface by a staggered structure. Therefore, we study the electron system considering a reduced first Brillouin zone of in-plane wave vectors. To this aim, we represent H^{el}_{test} with the $2N_z$ states

$$|k_x, k_y, i_z\rangle, \qquad |k_x + \pi, k_y + \pi, i_z\rangle, \tag{3.23}$$

with the wave vectors such that $-\pi/2 < k_x < \pi/2$, $-\pi/2 < k_y < \pi/2$, and i_z going from 1 to N_z. The eigenstates of electronic test Hamiltonian are indicated by $E(k_x, k_y, n)$, with the eigenvalue index n going from 1 to $2N_z$. The eigenvector related to n is specified in the following way: $b_{i_z}(\vec{k}_{||}, n)$ for the first N_z components, $p_{i_z}(\vec{k}_{||}, n)$ for the remaining N_z components.

The variational procedure is self-consistently performed by imposing that the total density of the system ρ is given by N_{La}/N_z, with N_{La} the number of layers of LMO block, and the local plane density $\chi(i_z)$ is equal to $\langle n_{\vec{R}_i} \rangle$. Therefore, one has to solve the following $N_z + 1$ equations:

$$\rho = \frac{1}{N_x N_y N_z} \sum_{\vec{k}_{||}} \sum_{n} n_F \left[E(\vec{k}_{||}, n) \right] \tag{3.24}$$

and

$$\begin{aligned}\chi(i_z) &= \frac{1}{N_x N_y}\sum_{\vec{k}_{||}}\sum_{n} n_F\left[E(\vec{k}_{||},n)\right] \\ &\Bigg[|b_{i_z}(\vec{k}_{||},n)|^2+|p_{i_z}(\vec{k}_{||},n)|^2+ \\ &[b^*_{i_z}(\vec{k}_{||},n)p_{i_z}(\vec{k}_{||},n)+p^*_{i_z}(\vec{k}_{||},n)b_{i_z}(\vec{k}_{||},n)]\Bigg],\end{aligned} \tag{3.25}$$

where $n_F(z)$ is the Fermi distribution function. These equations allow to obtain the chemical potential μ and the the local charge density $\chi(i_z)$. As result of the variational analysis, one is able to get the charge density profile corresponding to magnetic solutions which minimize the free energy.

3.2 Static properties and phase diagrams

We have found the magnetic solutions and the corresponding density profiles that are stable for different sizes of the LMO and SMO blocks. The inhomogeneous variational approach allows to determine the values of the electron-phonon parameters f_{i_z} and Δ_{i_z}, and the magnetic order of the t_{2g} spins through the effective magnetic fields h_{i_z}. We will study the systems in the intermediate to strong electron-phonon regime characteristic of manganite materials focusing on two values of coupling: $\lambda = 0.5$ and $\lambda = 0.8$. The maximum value of in-plane antiferromagnetic super-exchange is $\epsilon = 0.01t$. The value of the Coulomb term α is fixed to $\alpha = 0.2$. The heterostrucures will be analyzedin the low-temperature regime: $T = 0.05t$.

The general structure of the solutions is characterized by three phases running along z-direction. Actually, according to the parameters of the model, we find G or C antiferromagnetic phases corresponding to localized or delocalized charge carriers inside LMO block, respectively. The localization is ascribed to the electron-phonon coupling which gives rise to the formation of

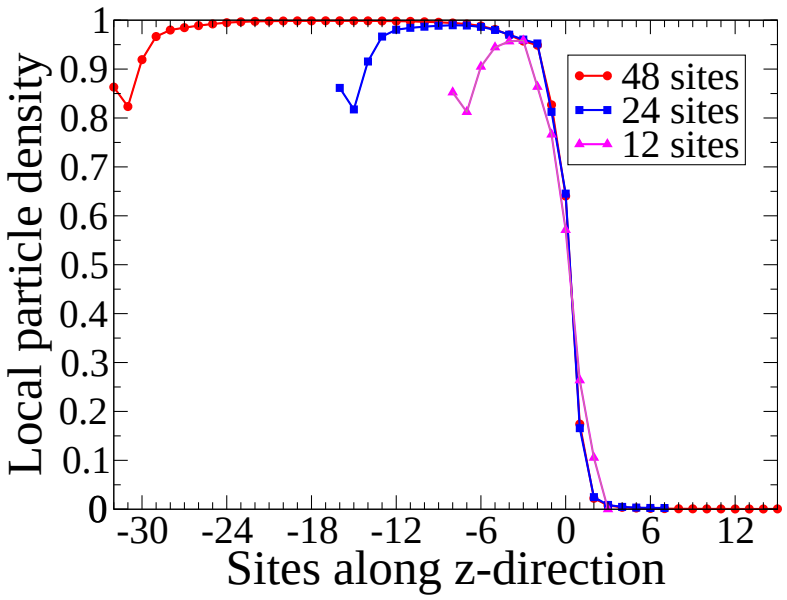

Figure 3.1: Comparison among density profiles corresponding to different sizes at $\lambda = 0.5$ and $\epsilon = 0.01t$. The index 0 indicates the interface Mn-plane between the last La-plane in LMO block and the first Sr-plane in SMO block.

small polarons. For the values of λ considered in this paper, a ferromagnetic phase always stabilizes around the interface. The size of the ferromagnetic region at the interface is determined by the minimization of the free energy and depends on the values of the system parameters. Only for larger values of λ and ϵ, the possibility of interface ferromagnetism is forbidden. Inside the SMO block, a localized polaronic G-type antiferromagnet phase is always stable.

At first, the scaling of the static properties as function of the size of the system along the z growth direction, has been analized. Therefore, a comparison of the density profiles has been done with $(LMO)_8/(SMO)_4$, $(LMO)_{16}/(SMO)_8$ and $(LMO)_{32}/(SMO)_{16}$ systems. In Fig. 3.1, we show the density profiles in a situation where strain-induced anisotropy has not been introduced. It is worth noticing that we indicate the interface Mn-plane

between the last La-plane in LMO block and the first Sr-plane in SMO block with the index 0. For a sufficiently large numbers of planes, the charge profile along z shows a well-defined shape. Indeed, the local density is nearly unity in LMO block, nearly zero in SMO block, and it decreases from 1 to 0 in the interface region. The decrease of charge density for the first planes of LMO is due to the effect of open boundary conditions along the z direction. In the intermediate electron-phonon coupling regime that we consider in Fig. (3.1), the region with charge dropping involves $4-5$ planes between the two blocks. We notice that the local charge density for $(LMO)_{16}/(SMO)_8$ and $(LMO)_{32}/(SMO)_{16}$ systems are very similar around the interface. Furthermore, the numerical results show close values of variational free energy corresponding to above mentioned systems. Given the similarity of the properties of these two systems, in the following, we will develop the analysis on the role of interface studying the system $(LMO)_{16}/(SMO)_8$.

For the same set of electron-phonon and magnetic couplings, the variational parameters and the Hartree self-consistent potential along z-axis are shown in Fig. 2. The effective magnetic fields are plotted for the most stable magnetic solution: antiferro G orders well inside LMO (planes $1-15$) and SMO (planes $19-24$), and ferromagnetic planes at the interface (planes $16-18$). The peak in the plot of the magnetic fields signals that ferromagnetism is quite robust at the interface. The variational electron-phonon parameters f_{i_z} are small on the LMO side and at the interface, but close to unity in SMO block. This means that, for these values of the couplings, carriers are delocalized in LMO up to the interface region, but small polarons are present in the SMO block. The quantities Δ_{i_z}, entering the variational treatment of the electron-phonon coupling, are determined by f_{i_z} and the local density $< n_{i_z} >$ through the equation: $\Delta_{i_z} =< n_{i_z} > (1 - f_{i_z})$. The Hartree self-consistent potential Φ indicates that charges are trapped into a potential well corresponding to the LMO block. Moreover, it is important to stress the energy scales involved in the well: the barrier between LMO and SMO block is of the order of the electron band-width. Furthermore, at the

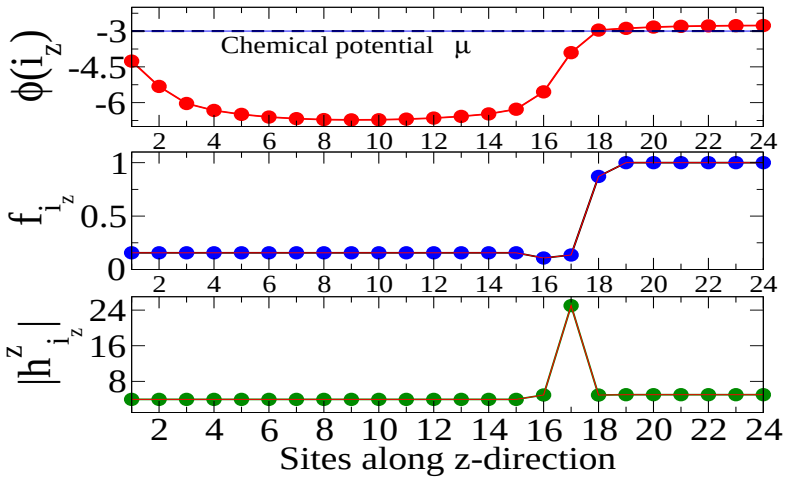

Figure 3.2: Self-consistent Hartree potential $\phi(i_z)$ (upper panel, in units of t), variational parameters f_{i_z} (mid panel) and effective magnetic fields $|h^z_{i_z}|$ (lower panel) along the z-axis for $\lambda = 0.5$ and $\epsilon = 0.01t$.

interface, the energy difference between neighboring planes is of the order of the hopping energy t.

As mentioned above, for these systems, strain plays an important role. In order to study quantitatively its effect, the phase diagram under the variation of the hopping anisotropy t_z/t has been investigated for two different values of ϵ_z ($\epsilon_z = \epsilon = 0.01t$, $\epsilon_z = 0$). Indeed, we simulate the compressive strain in the LMO block increasing the ratio t_z/t and decreasing ϵ_z/ϵ. On the other hand, the tensile strain in the SMO block favour the more isotropic $x^2 - y^2$ orbital and does not yield sizable effects. Therefore, for the SMO block, in the following, we choose $t_z = t$ and $\epsilon_z = \epsilon$. For what concerns the electron-phonon interaction, we assume an intermediate coupling, $\lambda = 0.8$. As shown in the upper panel of Fig. 3, with increasing the ratio t_z/t up to 1.7 for $\epsilon_z = \epsilon$, the magnetic order in LMO does not change since it remains G antiferromagnetic. However, the character of charge carriers is varied. Actually, for $\lambda = 0.8$, in the absence of anisotropy, small polarons are present in the LMO block. Moreover, at $t_z/t \simeq 1.5$, in LMO, a change from small localized polarons to large delocalized polaron occurs. For all values

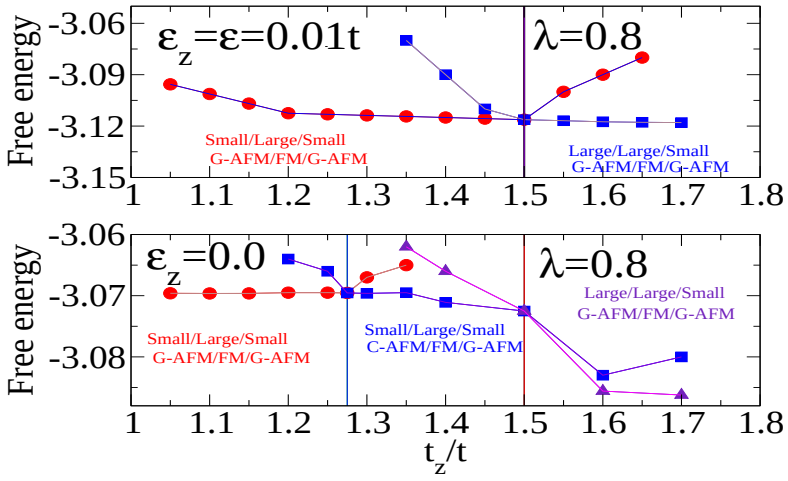

Figure 3.3: Phase diagram in the hopping anisotropy-energy plane for $LMO_{16}SMO_8$ system, corresponding to $\lambda = 0.8$ for $\epsilon_z = 0.01t$ (upper panel) and $\epsilon_z = 0$ (lower panel).

of the ratio t_z/t, the interface region is characterized by ferromagnetic order with large polaron carriers and SMO by G antiferromangnetic order with small polaron carriers.

It has been shown that it is also important to consider the anisotropy in super-exchange ($\epsilon_z \neq \epsilon$) parameters as consequence of strain. (32) In order to simulate the effect of compressive strain in LMO, a reduction of ϵ_z will be considered. We discuss the limiting case: $\epsilon_z = 0$. For this regime of parameters, the effect on the magnetic phases is the strongest. As shown in the lower panel of Fig. 3, for $1.28 \leq t_z/t \leq 1.5$, in LMO block, a C-type antiferromagnetic phase is the most favorable. The transition from small to large polaron again takes place at $t_z/t \simeq 1.5$. Therefore, we have shown that there is a range of parameters where LMO block has C-type antiferromagnetic order with small localized polarons. Due to the effect of strain, the magnetic solution in LMO turns out to be compatible with experimental results in superlattices. (15) The interface is still ferromagnetic with metallic large polaron features. In the figure $A/B/C$ refers to magnetic orders and character of charge carriers inside LMO (A), at interface (B),

inside SMO (C).

In order to analyze the effects of the electron-phonon interaction, a comparison between two different electron-phonon couplings is reported in Fig. 4. We have investigated the solutions which minimize the variational free energy at fixed value of the anisotropy factors $t_z/t = 1.3$ and $\epsilon_z = 0$ at $\lambda = 0.5$ and $\lambda = 0.8$. The magnetic solution in LMO block is C antiferromagnetic until the $15th$ plane. For both values of λ, polarons are small. In SMO block, starting from the $19th$ plane, the solution is G-type antiferromagnetic together with localized polarons. Three planes around the interface are ferromagnetically ordered. For $\lambda = 0.5$, all the three planes at the interface are characterized by delocalized polarons, while, for $\lambda = 0.8$, only the plane linking the ends of LMO and SMO blocks is with delocalized charge carriers.

As shown in Fig. 4, the quantity λ has important consequences on the physical properties such as the local particle density. Actually, for $\lambda = 0.8$ the transition from occupied to empty planes is sharper at the interface. Only one plane at the interface shows an intermediate density close to 0.5. For $\lambda = 0.5$ the charge profile is smoother and the three ferromagnetic planes with large polarons have densities different from zero and one.

For the analysis of the spectral and optical quantities, we will consider the parameters used for the discussion of the results in this last figure.

3.3 Spectral properties

In the following section the spectral properties of the heterostructure will be calculated for the same parameters used in Fig. 4.

Performing the canonical transformation (3.5) and exploiting the cyclic properties of the trace, the electron Matsubara Green's function becomes

$$\mathcal{G}(\vec{R}_i, \vec{R}_j, \tau) = -\langle T_\tau c_{\vec{R}_i}(\tau) X_{\vec{R}_i}(\tau) c^\dagger_{\vec{R}_j}(0) X^\dagger_{\vec{R}_j}(0)\rangle. \tag{3.26}$$

By using the test Hamiltonian (3.7), the correlation function can be disentangled into electronic and phononic terms. (58; 59) Going to Matsubara

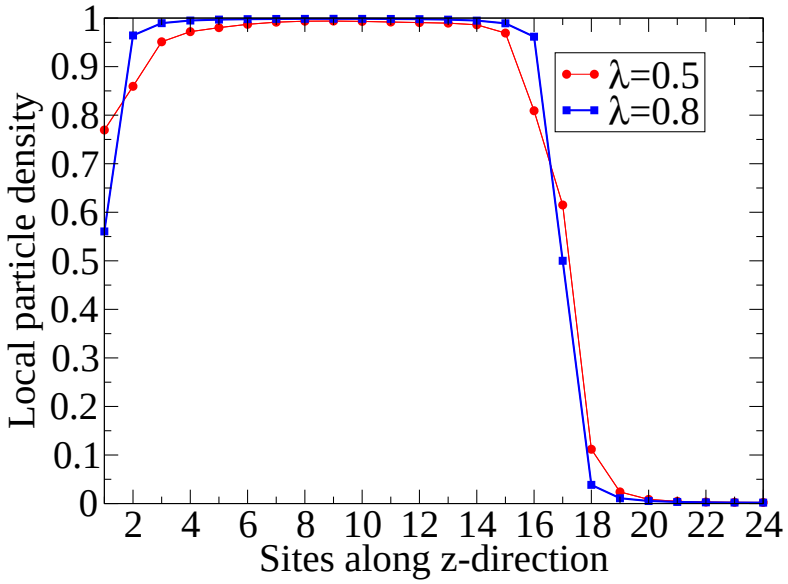

Figure 3.4: Comparison between local particle density corresponding to $\lambda = 0.5$ and $\lambda = 0.8$.

frequencies and making the analytic continuation $i\omega_n \to \omega + i\delta$, one obtains the retarded Green's function and the diagonal spectral function $A_{i_z}^{i_x i_y}(\omega)$ corresponding to $\vec{R}_i = \vec{R}_j$

$$\begin{aligned} &A_{i_z}^{i_x,i_y}(\omega) = \\ &e^{S_T^{i_z}} \sum_{l=-\infty}^{\infty} I_l(S^{i_z}) e^{\frac{\beta l\omega_0}{2}} [1 - n_F(\omega - l\omega_0)] g_{i_z}^{i_x,i_y}(\omega - l\omega_0) \\ &+ e^{S_T^{i_z}} \sum_{l=-\infty}^{\infty} I_l(S^{i_z}) e^{\frac{\beta l\omega_0}{2}} n_F(\omega + l\omega_0) g_{i_z}^{i_x,i_y}(\omega + l\omega_0), \end{aligned} \tag{3.27}$$

where $S_T^{i_z} = g^2 f_{i_z}^2 (2N_0 + 1)$, $S^{i_z} = 2g^2 f_{i_z}^2 [N_0(N_0 + 1)]^{\frac{1}{2}}$, $I_l(z)$ modified Bessel

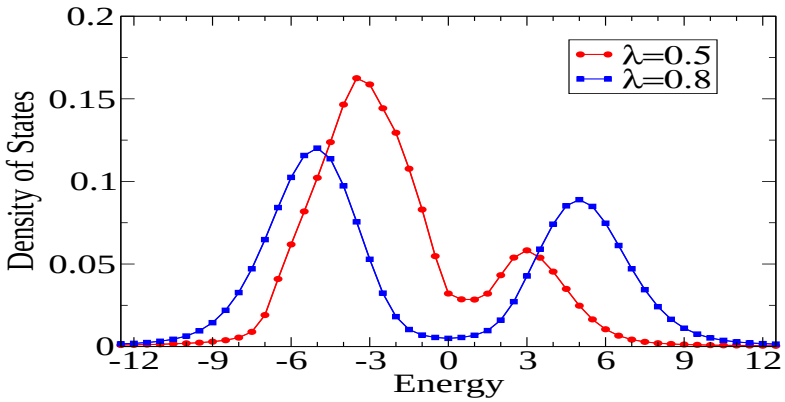

Figure 3.5: Comparison between density of states (in units of $1/t$) as a function of the energy (in units of t) corresponding to $\lambda = 0.5$ and $\lambda = 0.8$.

functions, and $g_{i_z}^{i_x,i_y}(\omega)$ is

$$g_{i_z}^{i_x,i_y}(\omega) = \frac{2\pi}{N_x N_y} \sum_{\vec{k}_{||}} \sum_{n=1}^{2N_z} \delta[\omega - E(\vec{k}_{||}, n)]$$
$$\times \Big[|b_{i_z}(\vec{k}_{||}, n)|^2 + |p_{i_z}(\vec{k}_{||}, n)|^2 +$$
$$(-1)^{i_x+i_y} [b_{i_z}^*(\vec{k}_{||}, n) p_{i_z}(\vec{k}_{||}, n) + p_{i_z}^*(\vec{k}_{||}, n) b_{ic_z}(\vec{k}_{||}, n)] \Big]. \tag{3.28}$$

The density of states $D(\omega)$ is defined as

$$D(\omega) = \frac{1}{N_x N_y N_z} \frac{1}{2\pi} \sum_{i_x,i_y,i_z} A_{i_z}^{i_x,i_y}(\omega). \tag{3.29}$$

In Fig. 5 is reported the density of state of the system $(LMO)_{16}/(SMO)_8$. It has been calculated measuring the energy to the chemical potential μ. This comparison has been made at fixed low temperature ($K_B T = 0.05t$), therefore we can consider the chemical potential very close to the Fermi energy of the system. At $\lambda = 0.5$, the spectral function exhibits a residual spectral weight at μ. The main contribution to the density of states at the chemical potential μ comes from the three ferromagnetic large polaron planes at the interface. Indeed, the contributions due to the (LMO) and (SMO) blocks is negligible.

For stronger electron-phonon coupling at $\lambda = 0.8$, it has been observed an important depression of the spectral function at μ. Hence the formation of a clear pseudogap takes place. This result is still compatible with the solution of our variational calculation since, for this value of $\lambda = 0.8$, there is only one plane with delocalized charge carriers which corresponds to the plane indicated as the interface ($i_z = 17$), while the two further ferromagnetic planes around the interface are characterized by small polarons. The depression of the density of the states at the Fermi energy is due also to the polaronic localization well inside the LMO and SMO block. In any case it is found that, even for $\lambda = 0.8$, the density of states never vanishes at the interface in agreement with experimental results. (13)

In this section it is found strong indications that a metallic ferromagnetic interface can form at the interface between LMO and SMO blocks. This situation should be relevant for superlattices with $n \geq 3$, where resistivity measurements made with contacts on top of LMO show a globally insulating behavior. In this analysis it has completely been neglected any effect due to disorder even if, both from experiments (10; 11) and theories (33), it has been suggested that localization induced by disorder could be the cause of the metal-insulator transition observed for $n \geq 3$. We point out that the sizable source of disorder due to the random doping with Sr^{2+} is strongly reduced since, in superlattices, La^{3+} and Sr^{2+} ions are spatially separated by interfaces. Therefore, the amount of disorder present in the heterostructure is strongly reduced in comparison with the alloy. However, considering the behavior of the LMO (SMO) block as that of a bulk with a small amount of holes (particles), one expects that even a weak disorder induces localization. On the other hand, a weak disorder is not able to prevent the formation of the ferromagnetic metallic interface favored by the double-exchange mechanism and the charge transfer between the bulk-like blocks: the states at the Fermi level due to the interface formation have enough density (13) so that they cannot be easily localized by weak disorder. In this section, it has been shown that this can be the case in the intermediate electron-phonon coupling regime

appropriate for LMO/SMO heterostructures.

In the next section it will be analyze the effects of electron-phonon coupling and strain on the optical conductivity in the same regime of the parameters considered in this section.

3.4 Optical properties

To determine the linear response to an external field of frequency ω, the conductivity tensor $\sigma_{\alpha,\beta}$ is derived by means of the Kubo formula. In order to calculate the absorption, the real part of the conductivity is calculated

$$Re\sigma_{\alpha,\alpha}(\omega) = -\frac{Im\Pi^{ret}_{\alpha,\alpha}}{\omega}, \tag{3.30}$$

where $\Pi^{ret}_{\alpha,\beta}$ is the retarded current-current correlation function. Following a well defined scheme (58; 59) and neglecting vertex corrections, one can get a compact expression for the real part of the conductivity $\sigma_{\alpha,\alpha}$. It is possible to get the conductivity both along the plane perpendicular to growth axis, σ_{xx}, and parallel to it, σ_{zz}. In order to calculate the current-current correlation function, one can use the spectral function $A_{\vec{k}_{||};i_z,j_z}$ derived in the previous section exploiting the translational invariance along in-plane direction. It is possible to show that the components of the real part of the conductivity become

$$\begin{aligned} Re[\sigma_{xx}](\omega) = \frac{e^2t^2}{N_xN_y}\sum_{k_x,k_y} 4sen^2(k_x)\frac{1}{N_z}\sum_{i_z,j_z}\gamma_{i_z}\gamma_{j_z} \\ \times\frac{1}{\omega}\int_{-\infty}^{\infty}\frac{d\omega_1}{4\pi}[n_F(\omega_1-\omega)-n_F(\omega_1)] \\ \times A_{k_x,k_y;i_z,j_z}(\omega_1-\omega)A_{k_x,k_y;i_z,j_z}(\omega_1), \end{aligned} \tag{3.31}$$

and

$$\begin{aligned} Re[\sigma_{zz}](\omega) = \frac{e^2t^2}{N_xN_y}\sum_{k_x,k_y}\frac{1}{N_z}\sum_{i_z,j_z}\sum_{\delta_{1z},\delta_{2z}}\delta_{1z}\delta_{2z} \\ \times\eta_{i_z,i_z+\delta_{1z}}\eta_{j_z,j_z+\delta_{2z}}\frac{1}{\omega}\int_{-\infty}^{\infty}\frac{d\omega_1}{4\pi}[n_F(\omega_1-\omega)-n_F(\omega_1)] \\ \times A_{k_x,k_y;i_z+\delta_{1z},j_z+\delta_{2z}}(\omega_1-\omega)A_{k_x,k_y;i_z,j_z}(\omega_1). \end{aligned} \tag{3.32}$$

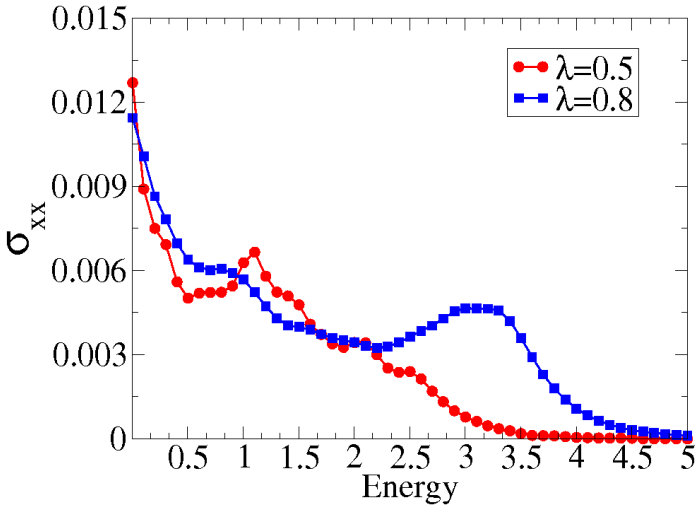

Figure 3.6: The conductivity (in units of $e^2/(mt)$, with $m = 1/(2t)$) into the plane perpendicular to growth direction of the $(LMO)_{16}/(SMO)_8$ bilayer as a function of the energy (in units of t) for different values of λ.

In Fig. 6, is reported the in-plane conductivity as function of the frequency at $\lambda = 0.5$ and $\lambda = 0.8$. We have checked that the in-plane response mainly comes from the interface planes. Both conductivities are characterized by a Drude-like response at low frequency. Therefore, the in-plane conductivity provides a clear signature of the formation of the metallic ferromagnetic interface. However, due to the effect of the interactions, it is found that the low frequency in-plane response is at least one order of magnitude smaller than that of free electrons in the heterostructures. Moreover, additional structures are present in the absorption with increasing energy. For $\lambda = 0.5$, a new band with a peak energy of the order of hopping $t = 2\omega_0$ is clear in the spectra. This structure can be surely ascribed to the presence of large polarons at the three interface planes. (58) Actually, this band comes from the incoherent multiphonon absorption of large polarons at the interface. This is also confirmed by the fact that this band is quite broad, therefore it can be interpreted in terms of multiple excitations. For $\lambda = 0.8$,

the band is even larger and shifted at higher energies. In this case, at the interface, large and small polarons are present with a ferromagnetic spin order. Therefore, there is a mixing of excitations whose net effect is the transfer of spectral weight at higher frequencies.

The out-of-plane optical conductivities show significant differences in comparison with the in-plane responses. In Fig. 7, is reported out-of-plane conductivity as function of the frequency at $\lambda = 0.5$ and $\lambda = 0.8$. First, it has been observed the absence of the Drude term. Moreover, the band at energy about $2\omega_0$ is narrower than that in the in-plane response. Therefore, the origin of this band has to be different. Actually, the out-of-plane optical conductivities are sensitive to the interface region. A charge carrier at the interface has to overcome an energy barrier in order to hop to the neighbour empty site. As shown in Fig. 2, the typical energy for close planes at the interface is of the order of the hopping t. Therefore, when one electrons hops along z, it has to pay at least an energy of the order of t. In the out-of-plane spectra, the peaks at low energy can be ascribed to this process. Of course, by paying a larger energy, the electron can hop to next nearest neighbors. This explains the width of this band due to inter-plane hopping.

Additional structures are present at higher energies in the out-of-plane conductivities. For $\lambda = 0.5$ the band at high energy is broad with small spectral weight. For $\lambda = 0.8$, there is an actual transfer of spectral weight at higher energies. A clear band is peaked around $10t$. This energy scale can be intepreted as given by $2g^2\omega_0 = 9.6t$ for $\lambda = 0.8$. Therefore, in the out-of-plane response, the contribution at high energy can be interpreted as due to small polarons. (58; 61)

Unfortunately, experimental data about optical properties of the LMO/SMO bilayers are still not available. Therefore, comparison with experiments is not possible. Predictions about the different behaviors among σ_{xx} and σ_{zz} can be easily checked if one uses in-plane and out-of-plane polarization of the electrical fields used in the experimental probes. More important, the formation of two-dimensional gas at the interface expects to be confirmed by

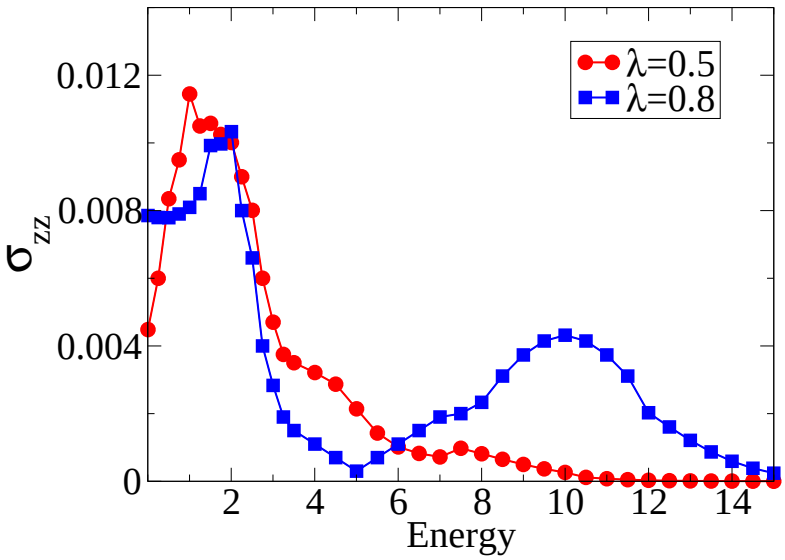

Figure 3.7: The conductivity (in units of $e^2/(mt)$, with $m = 1/(2t)$) along the growth direction of the $(LMO)_{16}(SMO)_8$ bilayer as a function of the energy (in units of t) for $\lambda = 0.5$ and $\lambda = 0.8$.

experiments made by using lateral contacts directly on the region between the LMO and SMO blocks. The d.c. conductivity of the sheet could directly measure the density of carriers of the interface metal and confirm the Drude-like low frequency behavior of in-plane response. Finally, one expects that a weak disorder present in the system and not included in our analysis can increase the scattering rate of the carriers reducing the value of the in-plane conductivity for $\omega \to 0$.

Conclusions

The elements of novelty of this thesis are the study of the effects induced by substrates on the ferromagnetic (FM) and transport properties in manganite thin films and the investigation to the role of the interface between two different insulating manganites.

The stability of MS phases in thin films of $La_{1-x}A_xMnO_3$ perovskites has been analyzed. A variational approach previously proposed for manganite bulk and films has been generalized in order to consider magnetically anisotropic phases. It is found that a reduction of the e_g electron hopping between nn sites, t, stabilizes a phase characterized by ferromagnetic planes perpendicular to the substrate with alternating up and down magnetizations. This phase exhibits an interesting *re-entrant* behavior shape into hopping-temperature plane determining, for suitable values of hopping, an interesting sequence of order-order transitions: FM$\mapsto$MS and MS$\mapsto$FM. Furthermore, the stability region moves toward larger values of the hopping amplitude as the number of the planes increases reaching saturation around 100 plane. All these results can have an interesting impact on a number of experimental results showing a strong anisotropy in the low-temperature resistivity of very thin films. In fact, the strain induced by the substrate triggers a decrease of the lattice parameter that, in turns, suggests a reduction of the in plane hopping. This is clearly understood for tensile strain but experimental data seem to indicate that it is true also for moderate compressive strain. As matter of fact, the calculated resistivity tensor in the *ab* plane shows an important anisotropy and reproduces the broad bump observed in the experiments at

around $100K$. This structure is due to re-entrant behavior of the MS phase and, therefore, is triggered by the double exchange mechanism. Indeed, in the range of temperatures where MS stabilizes, along the direction which presents anti-aligned t_{2g} spin, the resistivity decreases as temperature increases because the double-exchange effective hopping reduces. On the other hand, along the direction parallel to the stripes, the resistivity exhibits the expected metallic behavior.

It is worth noticing that all the results presented in this study have been obtained without assuming any extrinsic effect at the interface with the substrate. It is reasonable to believe that the possible existence of extrinsic effects can work as a further stabilizing factor for the MS phase. In the case of very thin films, the interplay between intrinsic and extrinsic effects can become stronger possibly giving rise to more complex magnetic patterns. The inclusion of the extrinsic effects in the analysis would require the proper study of the interface between film and substrate, that, in the present work, is taken into account in a average way assuming a reduction of the in-plane effective electron hopping.

Finally, it is important to note that in the present analysis the role of double exchange mechanism is studied at the level of variational mean-field that is able to grasp the main contribution able to stabilise the MS phases. Going beyond this approach would require to take into account the role of the scattering of electrons by magnons (64). This could affect the temperature profile of the resistivity, but not the anisotropy in different directions.

In the previous chapter phase diagrams, spectral and optical properties have been presented for a very large bilayer $(LMO)_{2n}/(SMO)_n$ (up to 48 sites along the growth direction). A correlated inhomogeneous mean-field approach has been developed in order to analyze the effects of electron-lattice anti-adiabatic fluctuations and strain. A metallic ferromagnetic interface is a quite robust feature of these systems for a large range of the electron-lattice couplings and strain strengths. Furthermore, the size of the interface region depends on the strength of electron-phonon interactions. At low temperature,

the general structure is characterized by three phases running along growth z-direction: antiferromagnetic phase with localized/Delocalized charge carriers inside LMO block, ferromagnetic state with itinerant carriers at the interface, localized polaronic G-type antiferromagnetic phase inside SMO block. The type of antiferromagnetic order inside LMO depends on the strain induced by the substrate.

Spectral and optical properties have been discussed for different parameter regimes. Due to the formation of the metallic interface, even in the intermediate to strong electron-phonon coupling regime, the density of states never vanishes at the chemical potential. Finally, in-plane and out-of-plane optical conductivities are sharply different: the former shows a metallic behavior, the latter a transfer of spectral weight at high frequency due to the effects of the electrostatic potential well trapping electrons in LMO block. The in-plane response provides a signature of the formation of the metallic ferromagnetic interface.

In this investigation focus has been on static and dynamic properties at very low temperature. The used approach is valid at any temperature. Therefore, it could be very interesting to analyze not only single interfaces, but also superlattices with different unit cells at finite temperature. Furthermore, in order to analyze the heterostructures in the regime of weak strain and in absence of orbital order, a double-orbital model should be adopted, for carefully treating the two e_g-like orbitals which make up Mn conduction band. Finally, it is worth noticing that the inclusion into the model of the disorder could work as a further factor to improve the comparison with experiments.

Acknowledgements

Ringrazio il Prof. Vittorio Cataudella per la guida ed il riferimento costante che ha rappresentato in questi anni.
Un ringraziamento carico di riconoscenza desidero indirizzarlo al Dr. Carmine Antonio Perroni, senza il quale non avrei ottenuto nessuno dei risultati conseguiti in questo lavoro di tesi.
Con affetto soltanto pari alla stima, ringrazio il Prof. Vincenzo Marigliano Ramaglia che, sin dai tempi del corso di laurea, è stato un modello al quale mi sono sempre ispirato nei giorni di forte motivazione.
Infine desidero ringraziare il Dr. Giulio De Filippis per la disponibilità che mi ha sempre riservato.

Bibliography

[1] A. Ohtomo and H. Y. Hwang, Nature (London) **419**, 378 (2002); S. Okamoto and A. J. Millis, Nature (London) **428**, 630 (2004).

[2] A. Ohtomo and H. Y. Hwang, Nature (London) **427**, 423 (2004) ; S. Thiel, G. Hammerl, A. Schmehl, C. W. Schneider, and J. Mannhart, Science **313**, 1942 (2006); N. Reyren , *ibid.* **317**, 1196 (2007).

[3] E. Dagotto, Nanoscale Phase Separation and Colossal Magnetoresistance (Springer-Verlag, Heidelberg, 2003).

[4] C. Zener, Phys. Rev. **81**, 440 (1951); C. Zener, **ibid. 82**, 403 (1951); P.W. Anderson and H. Hasegawa,

[5] A.J. Millis, Nature (London) **392**, 147 (1998).

[6] Mercone S et al. 2005 *Phys. Rev.* B **7**1 064415.

[7] Klein J, Philipp J B, Reisinger D, Opel M, Marx A, Erb A, Alff L and Gross R 2003 *J. of Appl. Phys.* **9**3 7373.

[8] Klein J, Philipp J B, Carbone G, Vigliante A, Alff L and Gross R 2002 *Phys. Rev. B* **6**6 052414.

[9] Orgiani et al. 2006 *Phys. Rev.* B **7**4 134419.

[10] A. Bhattacharya, S.J. May, S.G.E. Velthuis, M. Warusawithana, X. Zhai, B. Jiang, J.M. Zuo, M.R. Fitzsimmons, S.D. Bader, and J.N. Eckstein, Phys. Rev. Lett. **100**, 257203 (2008).

[11] C. Adamo, X. Ke, P. Schiffer, A. Soukiassian, M. Warusawithana, L. Maritato, and D.G. Schlom, Appl. Phys. Lett. **92**, 112508 (2008).

[12] N. Ogawa, T. Satoh, Y. Ogimoto, and K. Miyano, Phys. Rev. B **78**, 212409 (2008).

[13] S. Smadici, P. Abbamonte, A. Bhattacharya, X. Zhai, B. Jiang, A. Rusydi, J.N. Eckstein, S.D. Bader, and J.-M. Zuo, Phys. Rev. Lett. **99**, 196404 (2007).

[14] N. Ogawa, T. Satoh, Y. Ogimoto, and K. Miyano, Phys. Rev. B **80**, 241104(R) (2009).

[15] C. Aruta, C. Adamo, A. Galdi, P. Orgiani, V. Bisogni, N. B. Brookes, J.C. Cezar, P. Thakur, C.A. Perroni, G. De Filippis, V Cataudella, D.G. Schlom, L. Maritato, and G. Ghiringhelli, Phys. Rev. B **80**, 140405(R) (2009).

[16] H. Yamada, P.H. Xiang, and A. Sawa, Phys. Rev. B **81**, 014410 (2010).

[17] A. Iorio, C. A. Perroni, G. De Filippis, V. Marigliano Ramaglia, V. Cataudella, J. Phys.: Condens. Matter **21**, 456002 (2009).

[18] Huijben M, Martin L W, Chu Y-H, Holcomb M B, Yu P, Rijnders G, Blank D H A and Ramesh R 2008 *Phys. Rev.* B **7**8 094413.

[19] Luo Weidong, Pennycook S J and Pantelides S T 2008 *Phys. Rev. Lett* **1**01 247204.

[20] Dagotto Elbio, Hotta Takashi and Moreo Adriana 2001 *Physics Reports* **3**44.

[21] Dagotto E 2003 *Nanoscale Phase separation and Colossal Magnetoresistance* (Springer-Verlag, Heidelberg) p. 1

[22] A. Iorio, C. A. Perroni, V. Marigliano Ramaglia, and V. Cataudella, arXiv: 1011.5802v1 [cond-mat.str-el] (submitted to Phys. Rev. B)

[23] See the articles in the special issue, vol **288** of Science magazine.

[24] See, e.g. A. Gupta and J. Z. Sun, J. M. M. M. 24-43 (1999)

[25] C. Noguera, Physics and chemistry at oxide surfaces, (Cambridge University Press: Cambridge,1996)

[26] R. Hesper, et al., Phys. Rev. B62, 16046-16055 (2000)

[27] A. Georges et al., Rev. Mod. Phys., 68, 13 (1996)

[28] C. Adamo et al., Phys. Rev. B 79, 045125 (2009)

[29] A. J. Millis et al., Journal of Applied Physics 83, 1588 (1998)

[30] A. Biswas et al., Phys. rev. B, 63 184424 (2001)

[31] M. Izumi et al., Mat. Sci. Eng. B84 53-7 (2001)

[32] Z. Fang, I. V. Solovyev, and K. Terakura Phys. Rev. Lett. 84, 3169-3172 (2000)

[33] E. Dagotto, Science 318, 1076 (2007)

[34] S. Dong et al., Phys. Rev. B 78, 201102(R)(2008)

[35] B. R. K. Nanda and S. Satpathy, Phys. Rev. B 78, 054427 (2008)

[36] T. Z. Ward et al., Nature Phys. 5, 885 (2009)

[37] M. Uehara et al., Nature (London) 399, 560 (1999).

[38] M. Mayr et al., Phys. Rev. Lett. 86, 135 (2001)

[39] T. Z. Ward et al., Phys. Rev. Lett. 100,247204 (2008)

[40] S. Dong et al., Phys. Rev. B 82, 035118 (2010)]

[41] J. Gopalakrishnan et al., Phys. Rev. B 62, 9538-42 (2000)

[42] Y. Tomioka et al., Phys. Rev. B 61, 422 (2000)

[43] T. Koida et al., Phys. Rev. B 66, 144418 (2002).

[44] K. Maiti, P. Mahadevan, and D. D. Sarma, Phys. Rev. Lett. 80, 2885 (1998)

[45] S. Schwienger , M. Potthoff, and W. Nolting, Phys. Rev. B 67, 165408 (2003)

[46] A. Liebsch, cond-mat/0301418

[47] A. Liebsch, cond-mat/0301537

[48] D. M. Duffy and A. M. Stoneham, J. Phys. C 16 4087 (1983)

[49] S. Altieri et al., Phys. Rev. B 61, 16948 (2001)

[50] K. Maiti et al., Europhys. Lett. 55, 246 (2001)

[51] Zhang J, Bishop A R and Roder H 1996 *Phys. Rev.* B **53** 8840.

[52] Holstein T 1959 *Ann. Phys.* **8** 325; ibidem 1959 **8** 343.

[53] Perroni C A, De Filippis G, Cataudella V, and Iadonisi G 2001 *Phys. Rev.* B **64** 144302.

[54] Lang I J and Firsov Yu A 1963 *Soviet Physics JETP* **16** 1301; Firsov Yu A 1975 *Polarons* (Moskow, Nauka).

[55] Das A N and Sil S 1993 *J. Phys.: Condens. Matter* **5** 8265.

[56] Perroni C A, Cataudella V, De Filippis G, Iadonisi G, Marigliano Ramaglia V, Ventriglia F (2003) *Phys. Rev.* B **68** 224424.

[57] Shuai Dong, Seiji Yunoki, Xiaotian Zhang, Cengiz Sen, J.-M. Liu, and Elbio Dagotto, arXiv:1005.3865 (2010).

[58] C.A. Perroni, G. De Filippis, V. Cataudella, and G. Iadonisi, Phys. Rev. B **64**, 144302 (2001).

[59] C.A. Perroni, V. Cataudella, G. De Filippis, G. Iadonisi, V. Marigliano Ramaglia, and F. Ventriglia, Phys. Rev. B **68**, 224424 (2003).

[60] I.J. Lang and Yu. A. Firsov, Sov. Phys. JETP **16**, 1301 (1963).

[61] G. Mahan, *Many-Particle Physics*, 2nd ed. (Plenum Press, New York, 1990).

[62] von Helmolt A, Wecker J, Holzapfel B, Schultz L, and Samwer K 1993 *Phys. Rev. Lett.* **71** 2331; Jin S, Tiefel T H, McCormack M, Fastnacht R A, Ramesh R and Chen L H 1994 *Science* **264** 413.

[63] Zener C 1951 *Phys. Rev.* **81** 440; Zener C, 1951 *ibid.* **82** 403; Anderson P W and Hasegawa H 1955 *ibid.* **100** 675.

[64] Kubo K and Ohata N 1972 *J. Phys. Soc. Jpn.* **33**, 21.118 141.

[65] Millis A J, Littlewood P B and Shraiman B I 1995 **74**, 5144; Millis A J, Shraiman B I and Mueller R 1996 **77**, 175.

[66] Millis A J 1998 *Nature* **392** 147.

[67] Guo-Meng-Zhao, Coder K, Keller H, and Muller K A 1996 *Nature* **381** 676.

[68] Lanzara A, Saini N L, Brunelli M, Natali F, Bianconi A, Radaelli P G, and Cheong S W 1998 **81** 878.

[69] Kim K H, J. Gu JY, Choi H S, Park G W, and Noh T W 1996 **77** 1877.